Raman Spin-Lattice Relaxation of Shallow Donors in Silicon

THEODORE G. CASTNER, JR.
General Electric Research Laboratory, Schenectady, New York
(Received 26 October 1962)

This work reports both experimental measurements and calculations of two-phonon Raman spin-lattice relaxation times for shallow donors in silicon. Saturation, line broadening, and adiabatic fast passage techniques were used to measure T_s ($\Delta M_s=\pm1$, $\Delta M_I=0$) between 2 and 30°K for P, As, Sb, and Bi at 3300 G. T_x ($\Delta M_s=\pm1$, $\Delta M_I=\mp1$) was measured in the liquid He range for As, Sb, and Bi at 3300 G. The calculations of the spin-lattice relaxation rates $1/T_s$ and $1/T_x$ for Raman processes were made using only the $1S$ doublet and triplet valley-orbit excited states. The calculations were made for both the power-law temperature-dependent region and the exponential temperature-dependent region.

$1/T_s$ for P and As showed a power-law temperature dependence T^n with n closer to 9 than to 7 between 2.5 and 6°K for P and between 3 and 11°K for As. In this range there is no magnetic field-crystal axis orientation dependence and also no magnetic field dependence between 3300 and 8000 G as shown by Wilson and Feher. These facts suggest a spin-orbit spin-flip interaction which would have a "Van Vleck cancellation." No T^{13} Raman temperature-dependent $1/T_s$ was observed experimentally. P, As, Sb, and Bi all show an exponential temperature-dependent $1/T_s$ above 6, 11, 4, and 26°K, respectively. The rate constant E ($1/T_s-Ee^{-\Delta/kT}$) gets larger as one goes to the higher Z donor impurities.

The ratio T_s/T_x was measured between 2 and 5°K for As^{75}, the result showing $T_s/T_x\propto T^{-2}$ above 2.2°K consistent with $T_s\propto T^{-8.5}$ and $T_x\propto T^{-6.5}$ near 5°K. Experimental values of T_x were obtained for Sb^{121} and Bi^{209} at 2.2 and 4.2°K, respectively.

Use of the Hasegawa-Roth mechanism for the calculated Raman $1/T_s$ for both the power-law and the exponential temperature-dependent regions gives a result nearly four orders of magnitude smaller than experiment. In the short-wavelength phonon region the $1S$ triplet can be equally as important as the $1S$ doublet via intervalley Umklapp processes. For As it is shown that intervalley Umklapp processes will predominate over intravalley processes. In the exponential case the calculated $1/T_s$ rate can have a maximum value when the excited states have level widths equal $2g\mu_BH$.

The calculated Raman $1/T_x$ rates for the different donors show good agreement with the experimental values. The $1/T_x$ rate can have an exponential temperature-dependent term but it will be much smaller than the T^7 term for the temperature range considered here.

Calculations have been made of the level widths of the P and As $1S$ excited states due to spontaneous phonon emission. It is shown for As that the dominant intervalley Umklapp spontaneous emission will be sharply peaked along the [100] axis.

I. INTRODUCTION

THE first measurements of the spin-lattice relaxation of donor electrons in silicon at liquid He temperatures by Honig[1] and others[2–4] showed extremely long spin-lattice relaxation times. Subsequent experimental studies by Feher and Gere,[5] Honig and Stupp,[6] and Wilson and Feher[7] have produced quantitative data on the dependence of these relaxation times on temperature, magnetic field, magnetic field orientation with respect to the crystal axis, concentration of donor impurities, and the density of free electrons in the conduction band introduced by light. The temperature dependence of the relaxation rate (1.2 to 4.2°K) indicated a change from a linear temperature dependence associated with a single-phonon direct process, to a T^7 dependence, associated with a two-phonon Raman scattering process. For phosphorus, this T^7 process takes over above 2.5°K. Early theoretical attempts[8,9] to explain the long relaxation times were not very successful. More recently, Hasegawa[10] and Roth[11] independently developed a theory which gave excellent agreement with experiment for the single-phonon T_s process ($\Delta M_s=\pm1$, $\Delta M_I=0$). However, little effort has been made to explain the magnitude of the Raman relaxation.

The present work is concerned primarily with the temperature dependence of the spin-lattice relaxation between 2 and 30°K and is a study of two-phonon processes. The initial motivation for this work resulted from (1) a measurement[5] showing that the T_s measured at 20°K was more than three orders of magnitude shorter than predicted by an extrapolation of the T^{-7} dependence; (2) Abrahams' calculated T^{13} Raman process temperature dependence[9]; and (3) the fact that the important physical parameters and wave functions for silicon donors were well known, this suggesting that accurate relaxation rate calculations might be made. During the study the investigation was greatly stimulated by the experimental discovery[12] of an exponential temperature dependence for spin-lattice relaxation. The work of Hasegawa[10] and Roth,[11] showing for the first time the importance of the valley-

[1] A. Honig, Phys. Rev. **96**, 234 (1954).
[2] A. Honig and J. Combrisson, Phys. Rev. **102**, 917 (1956).
[3] A. Abragam and J. Combrisson, Compt. Rend. **243**, 576 (1956).
[4] G. Feher, R. C. Fletcher, and E. A. Gere, Phys. Rev. **100**, 1784 (1955).
[5] G. Feher, D. K. Wilson, and E. A. Gere, Phys. Rev. **114**, 1245 (1959).
[6] A. Honig and E. Stupp, Phys. Rev. **117**, 69 (1960).
[7] D. K. Wilson and G. Feher, Phys. Rev. **124**, 1068 (1961).
[8] D. Pines, J. Bardeen, and C. P. Slichter, Phys. Rev. **106**, 489 (1957).
[9] E. Abrahams, Phys. Rev. **107**, 491 (1957).
[10] H. Hasegawa, Phys. Rev. **118**, 1523 (1960).
[11] L. M. Roth, Phys. Rev. **118**, 1534 (1960).
[12] C. B. P. Finn, R. Orbach, and W. P. Wolf, Proc. Phys. Soc. (London) **77**, 261 (1960).

orbit splitting for spin-lattice relaxation, was a second important stimulant.

The suggestion[13] of an exponential temperature dependence for spin-lattice relaxation led to a fit with preliminary saturation data for T_s between 10 and 20°K for P donors in silicon. The slope yielded an activation energy of about 11×10^{-3} eV, in good agreement with the calculated position[14] of the $1S$ doublet and triplet above the $1S$ singlet ground state for the P donor. In previous work[15] the spin-lattice relaxation times for P, As, Sb, and Bi donors were measured over a temperature range and an exponential temperature dependence was found for each donor. The valley-orbit splittings were determined for these donors, the results indicating the $1S$ doublet and triplet energy levels were 34×10^{-3} eV below the conduction band minima for all the different donors. The exponential temperature-dependent spin-lattice relaxation for shallow donors in silicon is not surprising since the maximum phonon energies are several times larger than the energy splitting of the low-lying excited states above the donor ground state. However, unlike some rare-earth ions[12] the shallow donors also exhibit the usual power law (T^7 or T^9) temperature dependence for Raman spin-lattice relaxation.

Several questions arise concerning this exponential relaxation. (1) Is the anisotropic Zeeman interaction of the $1S$ doublet, used by Hasegawa[10] and Roth[11] as the spin-flipping interaction, able to account for the magnitude of the relaxation rate? (2) How does the calculated spin-lattice relaxation rate compare with Orbach's calculations[16] for the rare-earth paramagnetic ions? (3) The wavelengths of the "resonant" phonons vary from 10 to 25 Å which is equal to or less than the donor electron orbital radii. What new features appear when the usual long-wavelength approximation used for the orbit-lattice interaction matrix elements is poor. Calculations of the two-phonon spin-lattice relaxation are made using the Van Vleck[17] approach. These calculations are developed in Sec. VI and compared with those of Hasegawa and Roth.

Several interesting unanticipated results were found, namely, (1) in the short-wavelength phonon region not only the $1S$ doublet, but also the $1S$ triplet contributes to the spin-lattice relaxation. The relaxation via the $1S$ triplet states is a result of an intervalley scattering Umklapp process which, for the right magnitude of valley-orbit splitting, can predominate over the normal intravalley process. For As this dominance of the Umklapp intervalley over the intravalley relaxation appears to be supported by the experimental data. (2) The level broadening of the $1S$ excited states has an important effect on the magnitude of the relaxation in a way not present in Orbach's results. This dependence on level broadening can result in a maximum possible relaxation rate for a given magnitude of a spin-flipping interaction.

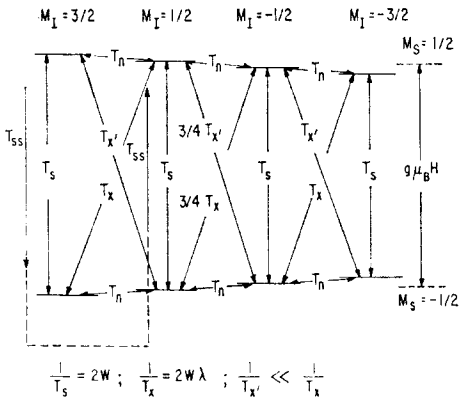

FIG. 1. Ground-state spin energy levels for As donors in silicon with $S=1/2$, $I=3/2$ for a large Zeeman splitting and a much smaller hyperfine splitting. The arrows show the various spin-lattice relaxation processes. In these experiments only the allowed transitions ($\Delta M_s=\pm1$, $\Delta M_I=0$) are excited with the microwave power.

As a by-product of these calculations some observations on the decay of donor electrons in excited donor states are made in Sec. VII. The generation of high-energy phonons by the decay of donor electrons in excited states is briefly analyzed, the result showing that the emitted phonons, as a result of Umklapp decay, have highly directional properties, the propagation vectors lying nearly along the [100] crystal axis.

II. THE VARIOUS RELAXATION PROCESSES

We consider As as a typical donor having an unpaired electron with $S=1/2$ interacting with a nucleus with $I=3/2$. Figure 1 shows the different energy levels of such a system with a small hyperfine splitting superimposed on a large Zeeman splitting. The various T_i represent the various spin-lattice relaxation processes. These processes have times T_s ($\Delta M_s=\pm1$, $\Delta M_I=0$), T_x ($\Delta M_s=\pm1$, $\Delta M_I=\mp1$), and T_n ($\Delta M_s=0$, $\Delta M_I=\pm1$). The other "diagonal" relaxation $T_{x'}$ ($\Delta M_s=\pm1$, $\Delta M_I=\pm1$) is negligible as has been shown experimentally.[6] No $T_{x'}$ relaxation is expected if the lattice waves only modulate the magnitude of an isotropic hyperfine interaction.

Exchange relaxation processes[5,18] (exchange between two donor electrons, exchange between a donor electron and a conduction electron, and also the interchange of a donor electron between two donor sites) designated by T_{ss} can also be important when the population differences of the different hyperfine lines are not equal to the Boltzmann values or to one another. If the concentration of donors is small enough ($n_D<10^{16}$/cc)

[13] The author is indebted to W. P. Wolf for pointing out the possibility of exponential temperature-dependent spin-lattice relaxation when there are low-lying excited states.

[14] W. Kohn and J. M. Luttinger, Phys. Rev. **97**, 1721 (1955); **98**, 1915 (1955).

[15] T. G. Castner, Jr., Phys. Rev. Letters **8**, 13 (1962).

[16] R. Orbach, Proc. Phys. Soc. (London) **77**, 821 (1960); Proc. Roy. Soc. (London) **A264**, 458 (1961).

[17] J. H. Van Vleck, Phys. Rev. **57**, 426 (1940).

[18] R. S. Levitt and A. Honig, J. Phys. Chem. Solids **22**, 269 (1961).

and no light, visible or infrared, is incident on the sample, exchange processes will not be important at liquid-helium temperatures. In the liquid-hydrogen range there is a small number of free electrons, n, in the conduction band given by[19]

$$n \simeq 6.6\times 10^{15} T^{3/2}[(N_D-N_A)/N_A]e^{-E_i/kT}, \quad (1)$$

where N_D is the number of donors, N_A the number of acceptors, and E_i the ionization energy of the particular donor. For P donors with $E_i/k=540°$K, $N_D/N_A=10$, and $T=20°$K, $n=10^7$/cc. This is about the same number of free carriers as Feher introduced with light at helium temperatures. However, the spin-lattice relaxation of the conduction electrons is slow[20] and the spin heat capacity of the 10^7 free electrons is small compared to the 10^{16}/cc donor electron spins having a T_s of 0.5 μsec at 20°K. Consequently, even though saturation of a single hyperfine line raises the spin temperature of that hyperfine line relative to the other hyperfine lines, the exchange-relaxation process is much too weak, compared to the T_s process, to spread the saturation to the other hyperfine lines. For As and Bi, experiments were done up to 30°K, but for these donors the E_i values are correspondingly higher and the resulting values of n are no larger.

Rate equations for the populations of the hyperfine levels have been solved[21] for the steady-state condition with the times T_s, T_x, and T_n as the relaxation processes for the case of microwave power applied to one of the allowed hyperfine line transitions. These solutions were obtained for the case $g\mu_B H \ll kT$ and for the hyperfine splitting negligible compared to the Zeeman splitting. Although there are several parallel paths for relaxation, if $T_n \gg T_s$ only the vertical relaxation ($\Delta M_I=0$) is important and each hyperfine line will have the same $T_{1\text{eff}} \simeq T_s$ independent of the relative magnitude of T_n and T_x. Experimentally, for P donors at helium temperature, $T_n \geq 30\, T_s$. Since the temperature dependence of the T_n process is not likely to be any stronger than that of the T_s process, then the above condition should continue to hold at liquid-hydrogen temperatures. For the other donors it will also be assumed that $T_n \gg T_s$ and that saturation of a given hyperfine line will determine T_s.

Culvahouse and Pipkin[22] have measured T_s and T_x for As^{75} by observing the recovery rates of the different hyperfine lines after inverting all the hyperfine lines by adiabatic fast passage. Their results yielded a different value of T_s/T_x at 4.2°K than at 1.3°K at 8500 G. In this work the ratio T_s/T_x was measured as a function of temperature. To interpret the data, computer calculations were made of the recovery of the individual hyperfine lines after inversion considering only T_s and T_x processes. The effect of a long T_n is quite unimportant when all the lines have been inverted. These results are discussed in Sec. VC.

III. TEMPERATURE DEPENDENCE OF SPIN-LATTICE RELAXATION

At low temperatures ($T<0.05\times\theta_D$, the Debye temperature) where $g\mu_B H \ll kT$, the spin-lattice relaxation time T_s of donor electrons in silicon can be represented by the empirical formula

$$1/T_s = AH^4T + BH^2T^7 + CT^9 + DT^{13} + E(H)e^{-\Delta/kT}, \quad (2)$$

where the magnetic field dependence is explicitly shown. The constants A through D contain deformation potentials, velocities of sound, etc., and also may contain an angular dependence (between H and the crystal axis). The first linear term is due to a single-phonon absorption or emission process (phonon energy $\hbar\omega = g\mu_B H$). All the other terms represent two-phonon Raman scattering processes and contain an integration over all phonon energies up to $k\theta_D$ with the restriction that the difference in energy of the absorbed and emitted phonon energies must equal the Zeeman energy. The T^7 term comes from a magnetic type of interaction, for example the anisotropic Zeeman interaction. Those phonons with energy within a few kT of $\hbar\omega \sim 6kT$ are most important for the T^7 term. The T^9 term results from the spin-orbit interaction as the spin-flipping mechanism, the higher temperature dependence coming from the well-known Van Vleck cancellation.[17] One should note that the T^7 term contains an H^2 field dependence while the T^9 term is independent of magnetic field. Abrahams[9] calculated a Raman process considering only dilatational deformations, which because of extra phase cancellations yielded a T^{13} temperature dependence also independent of magnetic field. However, Abrahams' calculated D coefficient is quite small because the long-wavelength dilatations couple only to different bands in higher order which are separated by several electron volts. The exponential term (Sec. VI D) results from a resonance fluorescence of phonons with energy $h\omega=\Delta$, where Δ ($\Delta<k\theta_D$) is the energy to the important excited states.

It is obvious from (2) that as one goes to high temperatures (T always less than $0.05\times\theta_D$) the temperature dependence of the spin-lattice relaxation rate can only go to the next higher term. For example, if the T^9 term follows the linear T term because of a small B coefficient, then the T^7 term will never be observed (fixed magnetic field). Similarly, with $\Delta \gg T$,

---

[19] See W. Shockley, *Electrons and Holes in Semiconductors* (D. Van Nostrand Company, Inc., Princeton, New Jersey, 1950), p. 472.

[20] G. Lancaster and E. E. Schneider, in *Proceedings of the International Conference on Semiconductor Physics, Prague, 1960* (Czechoslovakian Academy of Sciences, Prague, 1961). These authors show that for n-type samples (P, $n_D \sim 4\times 10^{17}$/cc) T_1 for the conduction electrons is about 2×10^{-8} sec at 100°K. At liquid-hydrogen temperature the conduction electron T_1 will be substantially longer.

[21] T. G. Castner, Jr., Ph.D. thesis, University of Illinois (unpublished).

[22] J. W. Culvahouse and F. M. Pipkin, Phys. Rev. **109**, 319 (1958).

if the exponential term were large and followed the linear term, one would not observe any of the power law Raman terms. This is the case for some paramagnetic rare-earth ions.[12] For the shallow donors in silicon the exponential relaxation starts at higher temperatures allowing the power law terms to sandwich between the linear term and the exponential term. One objective of the theory will be to determine correctly the values of all the coefficients in (2).

The phonon modulation of the isotropic hyperfine interaction produces a relaxation rate $1/T_x$ given by

$$1/T_x = aA_{\rm hf}^2H^2T + bA_{\rm hf}^2T^7, \qquad (3)$$

where $A_{\rm hf}$ is the magnitude of the hyperfine interaction (S-state contact term) and a and b are constants. The field dependence is two powers lower than for T_s processes. The possibility of an exponential temperature dependence for T_x is discussed in Sec. VI F.

The strong temperature dependence of Raman spin-lattice relaxation causes the relaxation times to very over many orders of magnitude from liquid-helium to liquid-hydrogen temperatures, typically from many seconds to small parts of a microsecond. In the next section we consider the methods to be used in measuring this range of times.

IV. EXPERIMENTAL METHODS AND APPARATUS

A. Methods of Relaxation Time Measurement Employed

1. *Saturation* (2×10^{-7} *sec* $< T_1 < 10^{-4}$ *sec*)

The spin resonance lines are inhomogeneously broadened with very narrow spin-packet widths much like the F center[23] in KCl. The spin-packet width has been measured[24] and gives a T_2 longer than 10^{-4} sec, therefore $T_2=T_1$ for T_1's shorter than 10^{-4} sec. Saturation measurements were readily made with an X-band spectrometer.[25] The onset of saturation of χ'', the absorption susceptibility, is a direct measure of T_1.

2. *Broadening of Inhomogeneous Line Envelope* ($T_1 < 10^{-8}$ *sec*)

At high temperatures, or high concentrations of donors, the relaxation time may become short enough so that the Lorentzian spin-packet width becomes comparable to or larger than the Gaussian inhomogeneous broadening. The resonance line broadens as T_1 gets shorter until finally the line shape will change to a Lorentzian. By measuring the Lorentzian component of the width one obtains T_1 (assuming $T_1=T_2$) by the relation

$$T_1 = (2/\sqrt{3}\gamma\Delta H_{\rm pp})K(a); \quad a=\Delta H_L/\Delta H_G, \qquad (4)$$

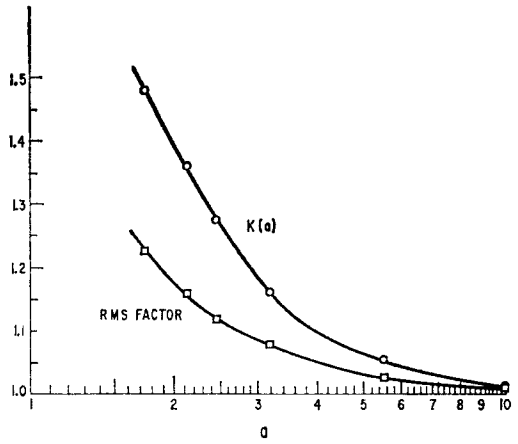

FIG. 2. $K(a)$ is the factor representing the ratio of the total peak-to-peak envelope width, $\Delta H_{\rm pp}$, to the Lorentzian spin-packet width, ΔH_L, for an inhomogeneously broadened line. a is the ratio of the Lorentzian spin-packet width, ΔH_L, to the Gaussian inhomogeneous broadening, ΔH_G. For $a>1$ $\Delta H_{\rm pp}$ may be used to determine T_1 directly.

where $\Delta H_{\rm pp}$ is the peak-to-peak width of the envelope; ΔH_L and ΔH_G are the Lorentzian and Gaussian widths, respectively; and $K(a)$ is a factor depending on the way one unfolds the Lorentzian and Gaussian from the actual line shape. $K(a)$ has been calculated and is compared in Fig. 2 with the result when one simply takes the rms sum of the Lorentzian and Gaussian contributions. For $a\sim1$ it is difficult to get accurate values of $K(a)$.

3. *Adiabatic Fast Passage Methods* ($T_1 > 10^{-3}$ *sec*)

This technique has been thoroughly discussed in the literature[26–28] and has been particularly useful for nuclear relaxation work.[29] We used a sweep large compared to the linewidth and observed the signal with a superheterodyne spectrometer and oscilloscope display. Since it is desirable to invert the population differences or the magnetization 100% on passage through the line, the following passage conditions must be carefully satisfied:

$$\begin{aligned} &\text{(a) Saturation} && \gamma H_1(T_1T_2)^{\frac{1}{2}} > 1, \\ &\text{(b) Adiabatic transitions} && \omega_m H_m \ll \gamma H_1^2, \\ &\text{(c) Fast passage} && \omega_m H_m \gg H_1/T_1, \\ &\text{(d) Spin diffusion} && \omega_m H_m \gg \Delta H/\tau_D. \end{aligned} \qquad (5)$$

H_m is the modulation amplitude, $\omega_m/2\pi$ is the modulation frequency, H_1 is the microwave magnetic field, ΔH is the total linewidth, and τ_D is the spin diffusion time. For T_1's$>10^{-3}$ sec, conditions (a) and (c) are easily satisfied. Condition (b), which is important for

[23] A. M. Portis, Phys. Rev. **91**, 1071 (1953).
[24] See J. P. Gordon and K. D. Bowers, Phys. Rev. Letters **1**, 368 (1958).
[25] T. G. Castner, Jr., Phys. Rev. **115**, 1506 (1959).
[26] F. Bloch, W. W. Hansen, and M. E. Packard, Phys. Rev. **70**, 474 (1946).
[27] L. E. Drain, Proc. Phys. Soc. (London) **A62**, 301 (1949).
[28] Ciaroti, Cristiani, Giulotto, and Lanzi, Nuovo Cimento **12**, 519 (1954).
[29] See for example, A. G. Redfield, Phys. Rev. **101**, 67 (1956).

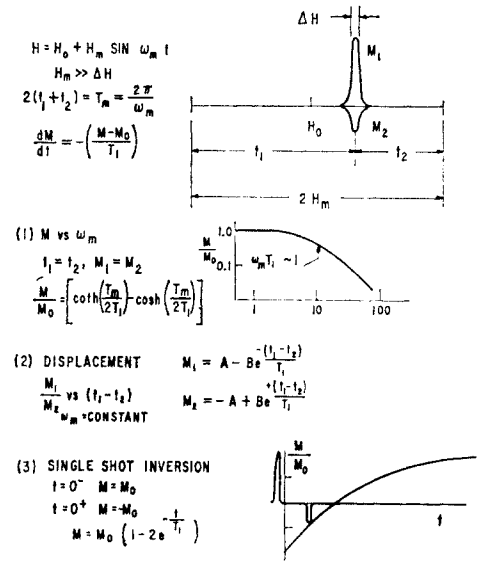

FIG. 3. Adiabatic fast passage methods of measuring T_1 when the magnetic field modulation amplitude or the field sweep is large compared to the linewidth. (1) In the M vs ω_m method the signal M starts to decrease as $\omega_m T_1$ approaches 1. (2) In the displacement method the ratio of the field-increasing signal M_1 to the field-decreasing signal M_2 vs (t_1-t_2) determines T_1. (3) The single shot inversion monitors the recovery at a variable time t after inversion at $t=0$.

complete population inversion during passage, is somewhat more difficult to satisfy depending on ω_m, T_1, and τ_D. Spin diffusion and forbidden transition effects[5] often play a role in preventing complete inversion. By careful choice of $\omega_m H_m$ and H_1 in the present work the loss of magnetization reversal per passage has been reduced to less than 2% for P and even less for As. The effects of spin diffusion and forbidden transitions on the loss of magnetization during each passage are not quantitatively understood at present. The loss of magnetization during passage must be known, however, to enable one to make valid measurements of T_1's.

Figure 3 shows the types of methods used in the fast passage region. For short times ($10^{-3} < T_1 < 0.3$ sec) the most convenient method is to measure the signal magnitude vs modulation frequency, $\omega_m/2\pi$. Displacement of the line position relative to the center of the field modulation changes the relative magnitude of the steady-state field-increasing and field-decreasing resonance signals. These relative magnitudes are readily found as a function of T_1, ω_m, and the displacement. The displacement method is most useful for the range 5×10^{-2} sec $< T_1 < 1$ sec. For very long times the usual single shot sweeps, with observations of the recovery a variable time later, are used to monitor the T_1's. Care was taken for the very long times to be certain that the microwave magnetic field was zero while the spins were relaxing and that no infrared radiation was incident on the sample.

B. Experimental Apparatus and Experimental Details

The saturation and the line broadening data were taken with an X-band spectrometer, previously described,[25] using balanced bolometer detection. For the fast passage work the spectrometer is converted to a 60-Mc/sec i.f. superheterodyne spectrometer. This is achieved by replacing the bolometers with crystals, introducing a modulator crystal between the V-58 klystron and the detector bridge magic tee. By driving the crystal with a 60-Mc/sec oscillator sidebands are obtained with about one mW/sideband. Two filter cavities, in series with phase shifters, follow the modulator crystal and reduce the carrier frequency and the other unneeded sideband by more than 60 dB. By this substitution one has a stable local oscillator using a single klystron already phase-locked to the carrier frequency. The output of the balanced-mixer bridge detector crystal is amplified by a 60-Mc/sec i.f. preamplifier and amplifier (100-dB gain) and is, then, fed to a balanced demodulator. A 60-Mc/sec reference voltage of the proper phase from the rf oscillator is fed to the demodulator. The dc output is displayed on an oscilloscope versus the field sweep voltage. This detection scheme is a phase coherent system capable of measuring χ' or χ'', and therefore can readily be used to measure the recovery of a resonance line after inverting it by adiabatic fast passage.

The temperature of the samples was varied from 2 to 30°K. The TE_{01} mode cavity is at the end of a 10-in. piece of thin-walled stainless steel waveguide section, all enclosed in a vacuum-tight can. Around each half of the split cavity is wound a heating coil. A carbon resistor is imbedded in one of the cavity walls. The sample is held pressed against a vertical narrow face by a block of styrofoam which fills the cavity. A thin film of apiezon grease is used to improve the thermal contact between the sample and the cavity wall. Helium exchange gas is used to regulate the amount of contact with the liquid refrigerant. With about 50 mW dissipated in the heater coils it is possible to maintain the cavity temperature at 12°K with liquid He and at 33°K with liquid H_2. By monitoring the temperature with the carbon resistor (Wheatstone bridge null method) it is easy to maintain a steady known temperature to approximately ½% of the absolute temperature. The carbon resistor was calibrated in the 2 to 4°K

TABLE I. Data on silicon samples.

Sample	Concentration number/cc	RT resistivity (Ω-cm)	Source
A	9×10^{15} P	0.70	Merck floating zone
B	3×10^{16} As	0.26	Czochralski grown
C	6×10^{16} Sb	0.15	Czochralski grown
D	4×10^{16} Bi	0.21	Czochralski grown
E	1.5×10^{15} P 2.5×10^{15} As	1.5	Czochralski grown

range and the 10 to 20°K range with vapor pressure-temperature curves. Particular care was taken to assure that the sample cavity was in good thermal contact with the solid hydrogen for temperatures between 10 and 14°K. Since the T_1 measurement accuracy is 5% or worse depending on the method, the $\frac{1}{2}$% temperature accuracy is sufficient despite the high power-law temperature dependences being studied.

The sample is placed on a cavity sidewall with a [110] crystal axis vertical; this arrangement helps shield the sample from any infrared leakage and also allows rotation of the magnetic field in a (110) plane covering the three principal directions [100], [110], [111]. A solid glass microwave quarter-wave plate was fitted snugly inside the waveguide above the cavity to reduce the infrared radiation getting to the cavity. Even at the lowest temperatures no shortening of the relaxation time due to infrared radiation was found.

A Hewlett-Packard low-frequency function generator is used to provide the variable frequency modulation for the fast passage work. For ν_m from 0.1 to 2 cps the output voltage is fed directly to the Varian magnet. For ν_m from 2 to 200 cps the function generator output is used to drive a dc power amplifier and a Helmholtz pair of modulation coils. $(\omega_m H_m)_{\max}$ could be 500 G rad/sec or larger, dependent on the modulation frequency. Typical H_1 values used for fast passage ranged from 0.007 to 0.07 G. With these values, it is possible to reasonably satisfy all the passage conditions in (5).

C. Samples

The Si samples used in this work are tabulated in Table I. Although the boron content is not specifically known, none of these samples is heavily compensated and it is likely that N_D/N_A for all these samples is substantially larger than ten.

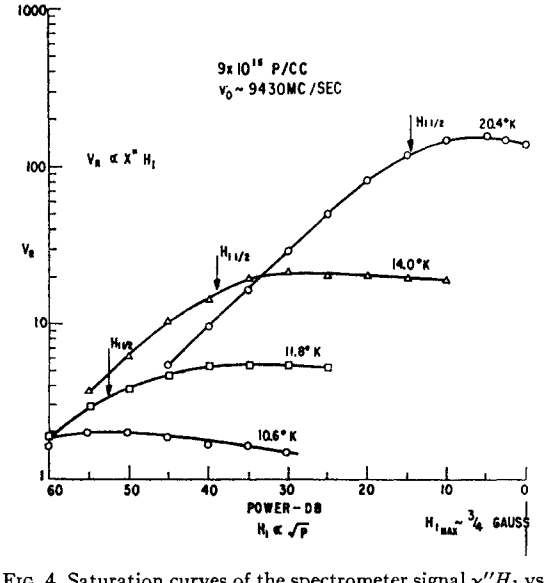

FIG. 4. Saturation curves of the spectrometer signal $\chi''H_1$ vs H_1, the microwave field, for P donors in Si (sample A) in the temperature range 10 to 20°K. The onset of saturation is a direct measure of T_1.

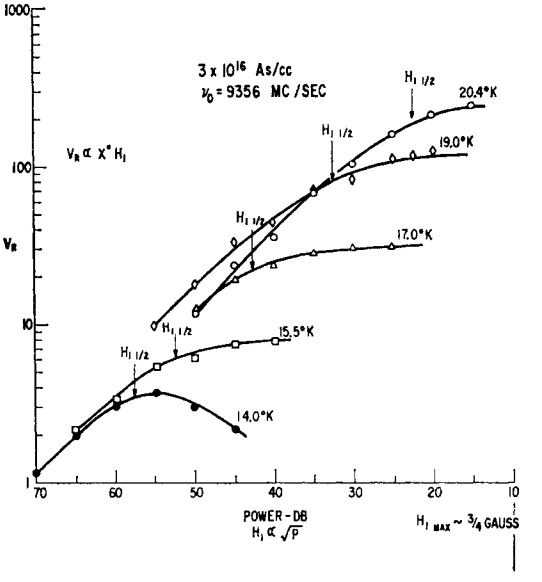

FIG. 5. Saturation curves of the spectrometer signal $\chi''H_1$ vs H_1 for As donors in Si (sample B) in the temperature range 14 to 20°K.

V. EXPERIMENTAL RESULTS AND DISCUSSION

A. Typical Data

Saturation curves are shown in Figs. 4 and 5 for P and As donors for a series of temperatures in the liquid-hydrogen range. At intermediate temperatures (14.0°K for P) the relative signal V_R ($V_R \propto \chi''H_1$) is linear below saturation and flattens as H_1 is increased, just as for the F-center case,[23] indicating the usual saturation behavior for inhomogeneously broadened lines when the spin-packet width is very much less than the Gaussian envelope width. Reducing the temperature, T_1 gets longer, approaching T_2',[24] the time associated with the static low-temperature spin-packet width. For $T_1 > T_2'$ the saturation curves bend down at high power and do not seem to behave like any of the calculated special passage cases. Spin diffusion would offer a qualitative explanation by spreading the saturation throughout the entire envelope, but this effect does not give quantitatively correct relaxation times. Nevertheless, at higher temperatures before the bend-over starts, an experimental measure of the onset of saturation, $H_{1\frac{1}{2}}$, is a direct measure of T_1. Very similar absorption saturation curves were observed for Sb and Bi donors although the temperature where the saturation occurs is very different for the two donors.

Figure 6 contains adiabatic fast passage data obtained for P donors, namely, a plot of the oscilloscope relative signal voltage vs magnetic field modulation frequency. The signal decreases as $\omega_m T_1$ approaches one. A

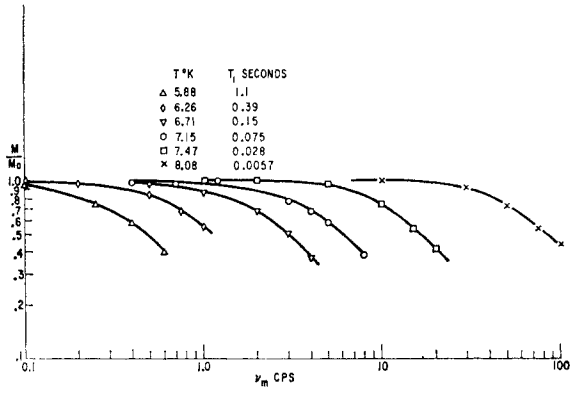

FIG. 6. Typical fast passage data for P donors using the M vs ω_m method for obtaining the T_1 values.

comparison of the experimental curves with the calculated curve gives T_1 directly. Sample E, containing small concentrations of both As and P donors, was run at 10°K, producing the recorder trace in Fig. 7. At 10°K the P donor has a much shorter T_1 than the As donor. The passage condition for the P lines is slow, the trace giving the slow passage dispersion derivative, while for As fast passage is amply satisfied ($H_1/\omega_m H_m = 8\times10^{-5}$ sec, $T_1=0.03$ sec), the trace showing the characteristic fast passage absorption envelope with opposite sign. The parameters and the signal for As correspond to Portis' case III-B.[30]

The four As hyperfine lines are readily inverted at helium temperatures. Recovery of the hyperfine lines after inversion is illustrated in Fig. 8. The ratio of the recovery of the two inner lines to the two outer lines determines T_s/T_x and then T_s and T_x may be determined from the individual rates. Below 2.5°K the times are so long that thermal equilibrium populations are difficult to achieve in convenient experimental times. This accounts for the deviation from Boltzmann

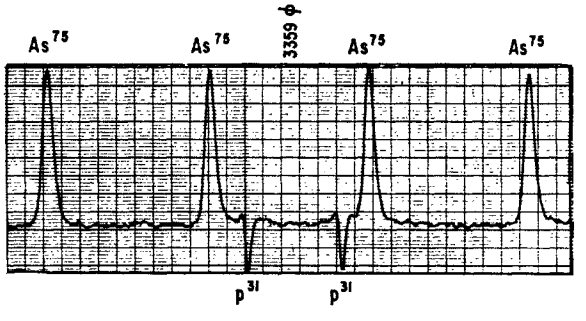

FIG. 7. Recorder electron spin resonance signal $\chi'H_1$ for sample E (2.6×10^{15} As/cc and 1.4×10^{15} P/cc) at 10.1°K. $H_1/\omega_m H_m \sim 8\times10^{-5}$ sec. The P^{31} shows a normal dispersion derivative signal indicating a short T_1, however the As^{75} dispersion signal resembles an absorption signal of opposite sign and represents a much longer T_1.

[30] A. M. Portis, "Magnetic Resonance in Systems with Spectral Distributions," Office of Scientific Research, Air Research and Development Command Report, 1955 (unpublished).

population difference at $t=0^+$. Figure 9 shows recovery curves after inversion of the Sb^{121} ($I=5/2$) and Sb^{123} ($I=7/2$) isotopes. One notes that the innermost lines recover most rapidly, the outermost lines most slowly. The Sb^{121} lines are recovering more rapidly than the Sb^{123} lines, consistent with the larger hyperfine splitting for Sb^{121}. Because of the short times and the high concentration of Sb donors needed for an adequate signal, not much effort was spent in obtaining accurate T_1's for the Sb isotopes in the helium range. For Bi^{209} ($I=9/2$) with a hyperfine splitting of 528 G it was not possible to invert more than a single line at a time. Since the Zeeman interaction isn't large compared to the hyperfine interaction and both T_s and T_x are complicated functions of magnetic field, it wasn't worthwhile to do much with Bi even though the T_1's were long enough for fast passage at 4.2°K.

Computer calculations of the recovery of the As^{75} hyperfine energy level populations after inversion were made at temperatures of 2.5, 2.0, and 1.5°K for a series of λ values. Figure 10 shows the various ratios (ratios characteristic of the average recovery of the two inner lines compared to the average recovery of the two outer lines) versus λ. The ratio of zero-crossing times [curve (b)] is similar to Culvahouse and Pipkin's curve[22] except that it starts to flatten slightly at large values of λ. Curve (c) is closest to a straight line and is the strongest function of λ. Neglecting experimental error considerations measurements of the slopes at

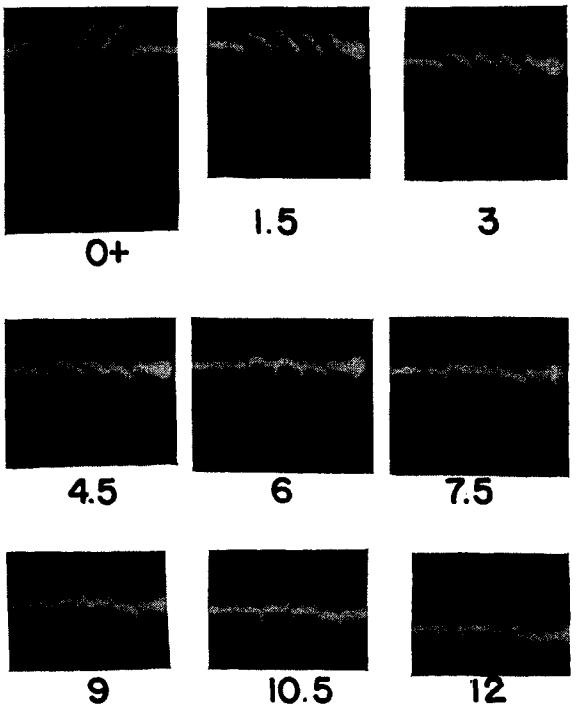

FIG. 8. The recovery of the four As hyperfine lines after inversion of all four lines at 2.44°K (times are in minutes). The unequal signal intensities of the four lines at $t=0$ is mainly a result of an inadequate wait in preparing thermal equilibrium populations.

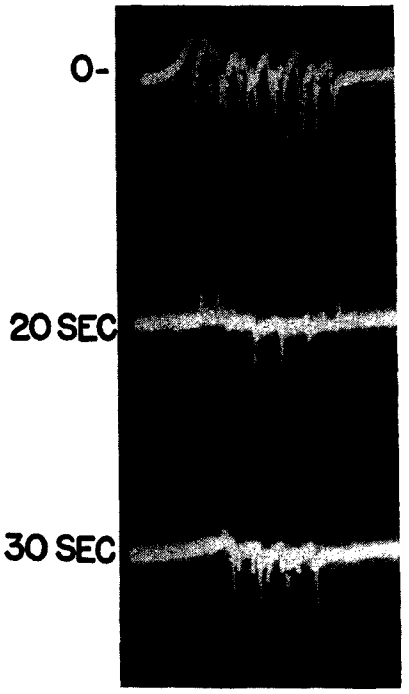

FIG. 9. The recovery after inversion at 2.50°K of the six Sb^{121} hyperfine lines and the eight Sb^{123} hyperfine lines. The Sb^{121} lines are recovering more rapidly than the Sb^{123} lines. For Sb^{121}, $T_x < T_s$ and the central lines are recovering most rapidly because of the dominant hyperfine spin-lattice relaxation.

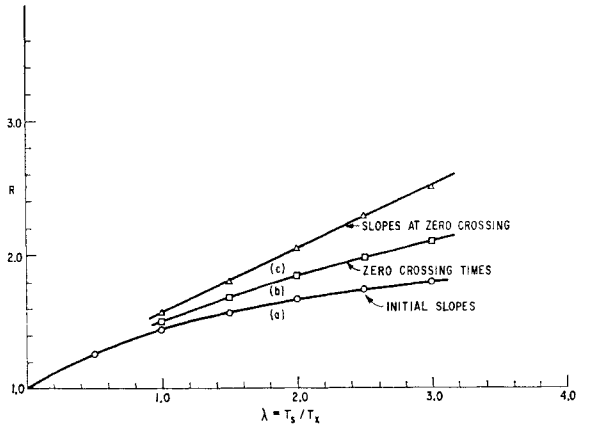

FIG. 10. Characteristic ratios of the rate of average recovery after inversion of the two inner lines to the average recovery of the two outer lines vs T_s/T_x. (a) is the ratio of the initial recovery slopes of the inner to the outer; (b) is the ratio of the average zero-signal crossing times of the outer to the inner; (c) is the ratio of the average inner slopes to the average outer slopes at the respective zero-crossing times.

zero crossing would give the most accurate values of λ. In practice, however, because of poor signal-to-noise near crossover and also errors which grow with time, the initial slope ratio and the time of crossover ratio give more accurate values of λ. Consistency of the three methods was used to ascertain the quality of the data points and to estimate limits of error.

B. T_s Results

The results of the T_s data for P, As, Sb, and Bi are given in Fig. 11. For Sb and Bi only good saturation data could be obtained. Good data were obtained for P over the entire temperature range, while for As more scatter is observed, particularly at low temperatures. For both P and As the relaxation time T_s varies inversely with the temperature up to 2.4 and 3.0°K, respectively, then goes into a power-law region. A line with a T^{-7} dependence is drawn between the P and As $\log T_s$ vs $\log T$ curves. Both P and As have slopes that are measurably steeper than the T^{-7} line and seem to be more closely parallel to the T^{-9} line shown in the figure. At 6 and 11°K, respectively, P and As begin exponential temperature-dependent relaxation. The exponential relaxation rates have been extended to lower temperature (see dashed lines) on the figure. One notes that at 5.1 and 9.2°K, respectively, for P and As the exponential relaxation is about 10% of the total rate; therefore, the effect of exponential relaxation on the slope in the power-law region is negligible below these temperatures. Our first important conclusion is that the power-law region is closer to a T^{-9} dependence rather than the T^{-7} dependence reported previously.[5,6] For P the power-law region (2.4 to 5.1°K) is too small to be very certain, but for As the power law region (3 to 9.2°K) is large enough to demonstrate the better fit

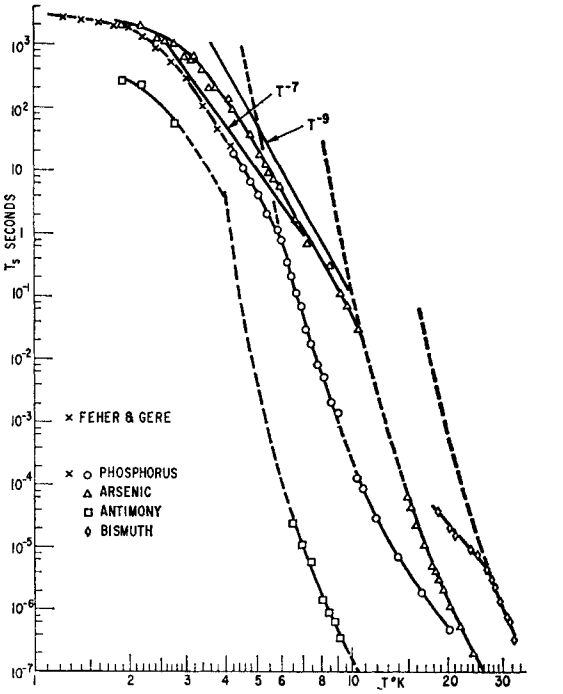

FIG. 11. T_s data for P, As, Sb, and Bi donors. The figure shows $\log T_s$ vs $\log T$, hence a constant slope indicates $T_s \propto T^{-n}$. T^{-7} and T^{-9} guide lines are shown. The high-temperature $T_s \propto e^{\Delta/kT}$ curves are extended with dashed lines into the power-law region to help show when the exponential contribution can be neglected.

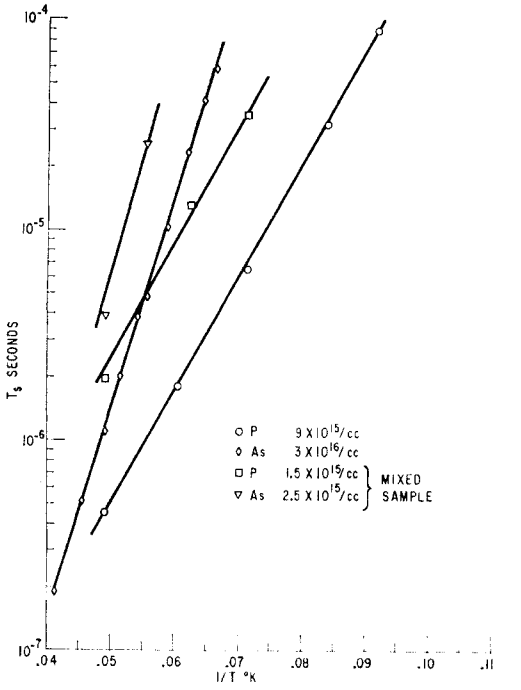

FIG. 12. Log T_s vs $1/T$ for P and As donors in samples A and B, respectively, and also the mixed (P and As) sample E. The results for the more dilute sample E indicate about the same slope, Δ/k, but a rate constant E ($1/T_s \propto Ee^{-\Delta/kT}$) smaller by a factor more than four for both P and As.

with the T^{-9} dependence. In addition, the lack of any field dependence[7] and the lack of any angular dependence at 4.2°K for the T_s of P point to the "Van Vleck cancellation" field-independent T^{-9} Raman term. This would suggest that the spin-orbit interaction is responsible for this relaxation. There is no experimental evidence for a T^{-13} temperature-dependent Raman term.

For Sb^{121} only the exponential range and a few tentative data points in the helium range are shown. It is estimated exponential relaxation would start in the vicinity of 4°K. For Bi the exponential relaxation changes to a power-law dependence close to 26°K; however, the slope is less than the T^{-9} and T^{-7} lines. The reason for this is that the long-wavelength approximation becomes poor for phonons with wave number q when qa^* approaches one (a^* is the donor electron orbital radius). For the T^9 term the most important phonons are transverse phonons with energy near $\hbar\omega = 8kT$ with a value of $qa^* \simeq 0.4T$. Breakdown of the long-wavelength approximation is already beginning at helium temperatures. This breakdown would also explain why the slopes for P and As are slightly less than -9.

Saturation runs were made on sample E with low concentrations of both P and As donors in the liquid-hydrogen range. Inadequate signal-to-noise didn't permit fast passage measurements at helium temperatures. The points are compared with samples A and B in Fig. 12. The less accurate T_s values obtained for sample E indicated exponential temperature-dependent relaxation with about the same slope[31] as the more heavily doped samples. For both P and As the relaxation rate is more than four times slower for the lightly doped samples. This concentration dependence is not very strong and may be similar to that found by Honig[6] for the direct single-phonon process. The significant result for this mixed sample is that the rate constant E [see Eq. (2)] for As is 75 times larger than for P. Moreover, the E's for Sb and Bi are, respectively, 4 and 8 times the As value. Although some of this variation may be due to the higher concentrations of Sb and Bi donors, it would appear that E depends strongly on the atomic number Z of the donor. One notes in the summary of the T_s results below in Table II that the rate constant C does not have the same strong Z dependence.

C. T_x Results

By observing the recovery of the four hyperfine lines of As^{75} (sample B) after inversion λ was measured between 2 and 5°K. The results in Fig. 13 demonstrate that, between 2.2 and 5°K and probably higher $\lambda \propto T^{-2}$. Below 2°K the data points of Abragam and Combrisson,[3] and Feher[8] suggest that $\lambda(T)$ flattens out at about 2. Below 2.2°K T_s and T_x are both inversely proportional to temperature (λ = constant), while above 2.2°K T_s decreases more rapidly with increasing temperature than T_x. Near 5°K $T_s \propto T^{-8.5}$ and $T_x \propto T^{-6.5}$ as shown in Fig. 14 of separate plots of T_s and T_x vs T.

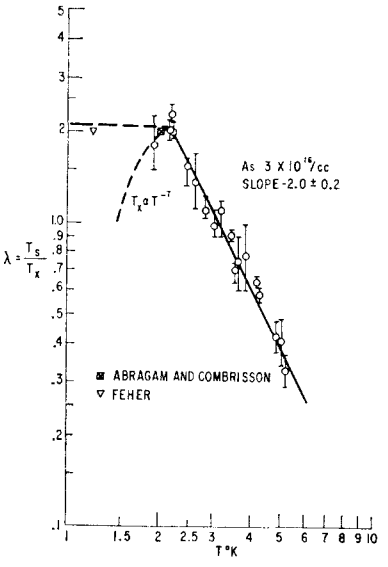

FIG. 13. Log(T_s/T_x) vs log$T$ for As donors in sample B. These values are all for $H \sim 3300$ G. Reference 22 contains values for $H \sim 8500$ G. Above 2°K $T_s/T_x \propto T^{-2}$.

[31] The ionization energy of shallow donors is concentration dependent [see P. P. Debye and E. M. Conwell, Phys. Rev. **93**, 693 (1954)]. Slightly larger slopes or valley-orbit splittings might be expected for sample E.

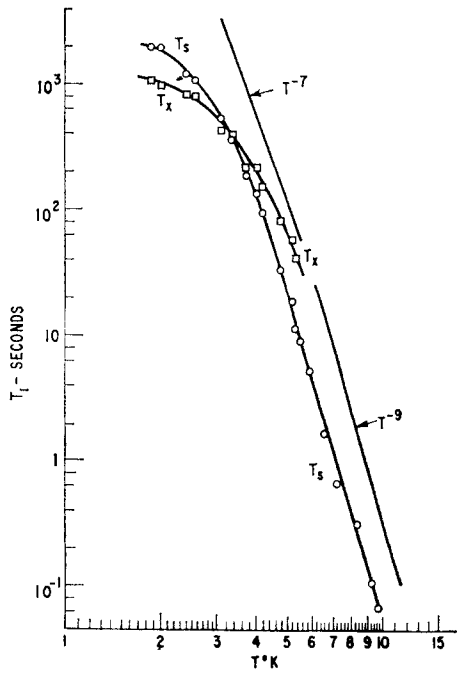

FIG. 14. LogT_s and logT_x vs log T for As donors in sample B at $H\sim3300$ G. Both T_s and T_x are into the Raman region above 3°K.

This lends additional support for the importance of the CT^9 Raman relaxation rate for $1/T_s$.

Culvahouse and Pipkin's experiments[22] were at 8500 G compared with our 3300 G. At the same temperature their single-phonon $1/T_s$ should be $(8.5/3.3)^4$ larger than ours and their single-phonon $1/T_x$ should be $(8.5/3.3)^2$ larger than ours. For their case the pure Raman region is probably not important until above 4.2°K. This is borne out by their smaller change in λ, $\lambda\simeq1$ to $\lambda\simeq1.5\pm0.5$, between 4.2 and 1.3°K. CP observed only a change of a factor of 6 in T_s between 4.2 and 1.3°K, while in this work there was a factor of 20 between 4.2 and 2°K. CP obtained $T_s=T_x=60$ sec at 4.2°K compared with the values here of $T_s\simeq100$ sec and $T_x\simeq170$ sec at 4.2°K. These values are not inconsistent, considering the different magnetic fields and the different magnetic field and temperature dependences of T_s and T_x. However, for the normal single-phonon process $1/T_s\propto H^4$ and $1/T_x\propto H^2$, hence $\lambda\propto H^{-2}$ at low enough temperatures. Our low-temperature value of $\lambda\simeq2$ is not consistent with CP's value of $\lambda\simeq1.5$. Although Honig[6] has found other single-phonon mechanisms with different field dependences for $1/T_s$ than H^4, the H^4 mechanism is expected to be dominant above 3000 G. Wilson and Feher[7] have discussed the sensitivity of a single-phonon T_x process to residual lattice strains. Different residual strains for CP's sample than for sample B would be a possible explanation for the lack of fit with $\lambda\propto H^{-2}$. The cause for the discrepancy is very uncertain.

In an experiment with Sb^{121} T_x was found to be approximately 100 sec at 2.2°K. For Bi T_x was found to be about 7 sec at 4.2°K. The T_x results in this section will be compared with theory and previous results in Sec. VI E.

TABLE II. T_s results.

Donor and sample	Conc. (10^{16}/cc)	Δ (°K)	Power law start (°K)	CT^9 C ($\sec^{-1}$ °K^{-9})	Expon. law start (°K)	$Ee^{-\Delta/kT}$ E (10^{10} $\sec^{-1}$)
P A	0.9	122.5	2.4	1.0×10^{-7}	6.0	0.091
P E	0.15	...	...	...	...	0.020
As B	3	229	3.0	2.0×10^{-8}	11	6.4
As E	0.25	...	...	...	...	1.5
Sb C	6	105	...	2×10^{-6}	4	26
Bi D	4	393	...	...	26	52

D. Summary of Experimental Conclusions

Above the linear temperature region $1/T_s\propto T^n$, where the evidence points to $n\simeq9$ in contrast to the T^7 dependence reported by Feher[5] and Honig.[6] At different temperatures, depending on the magnitude of the valley-orbit splitting Δ, all the donors start exponential temperature-dependent relaxation. The rate constant E, although slightly concentration dependent, seems to be strongly dependent on the atomic number Z of the donor. However, the rate constant C of the T^9 dependence does not follow the same Z dependence as E.

For As $T_s/T_x\propto T^{-2}$ between 2.2 and 5°K consistent with $T_s\propto T^{-8.5}$ and $T_x\propto T^{-6.5}$.

VI. RAMAN PROCESS SPIN-LATTICE RELAXATION CALCULATIONS

A. Introduction

Van Vleck's development,[17] using perturbation theory, of the calculation of spin-lattice relaxation rates will be the basis for the calculations made here and the calculations will be similar to those of Hasegawa[10] and Roth.[11] Orbach,[16] in his work on the rare-earth ions, has reviewed the historical developments and the present status of the spin-lattice relaxation field. Therefore, we start right in with the perturbation theory to be used.

The Hamiltonian for a donor electron in a silicon lattice can be written

$$H=H^0+H^1+H^{o1}, \tag{6}$$

where H^0 is the complete static Hamiltonian (including spin-orbit, hyperfine, Zeeman, and other interactions) for the donor electron in a rigid lattice, H^1 represents the Hamiltonian of quantized lattice waves, and H^{o1} is the weak interaction of orbital motion of the donor electron with the phonons. Because matrix elements of H^{o1} are very small compared with the diagonal energy splittings of H^0, we employ perturbation theory. It is convenient to start with an approximate separated

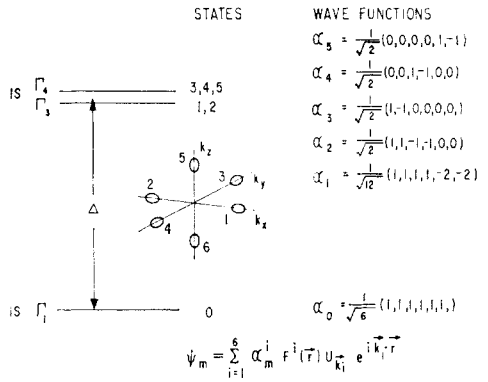

FIG. 15. Wave functions (after Kohn) for the 1S valley-orbit singlet, doublet, and triplet. The six degenerate conduction band valleys are also shown, the mimima resting about 15% in from the first Brillouin zone edges along [100] axis. The doublet and triplet are considered nearly degenerate at an energy Δ above the singlet.

wave function

$$\Psi(\mathbf{r},M_s,M_I,n_q)=\psi(\mathbf{r})\varphi_{M_s}\varphi_{M_I}\prod_{\mathbf{q}}\Phi_{n_q}(\mathbf{q}\cdot\mathbf{r}), \qquad (7)$$

which is only an approximate eigenfunction of H^0. We now divide H^0 into diagonal terms, $H^{\rm d}$, and non-diagonal terms, $H^{\rm nd}$, for the basis functions (7).

For the Raman two-phonon scattering process we utilize third-order perturbation theory using one $H^{\rm o1}$ for the absorption of a phonon and another $H^{*\rm o1}$ for the emission of a phonon and the part of $H^{\rm nd}$ producing the desired spin-flip, subject to the requirement of conservation of energy for the total system of electron spins plus phonons. The Raman transition probability will be

$$W_{j\leftarrow i}{}^{\rm Raman}=\frac{2\pi}{\hbar}\left|\sum_{k,m}\frac{H_{jm}H_{mk}H_{ki}}{(E_i-E_k)(E_i-E_m)}\right|^2\rho_{E_j}. \qquad (8)$$

We must use all possible permutations of H^{nd}, $H^{\rm o1}$, and $H^{*\rm o1}$.

Studies of the physical properties of shallow donors in semiconductors have been extensive and are reviewed by Kohn.[32] The conduction band minimum is sixfold degenerate with the minima on [100] axis about 85% out toward the edge of the first zone. The energy ellipsoids at each minimum are characterized by longitudinal and transverse effective masses and also by longitudinal and transverse g values (spectroscopic splitting factors), respectively, g_l and g_t. The donor wave functions are linear combinations of Bloch functions times hydrogenic envelope functions associated with the 6 conduction band minima. Each hydrogenic state has a sixfold degeneracy which can be removed by the tetrahedral crystalline field and the impurity potential. The wave functions for the low-lying states of a shallow donor are shown in Fig. 15.

[32] W. Kohn in *Solid State Physics*, edited by F. Seitz and D. Turnbull (Academic Press Inc., New York, 1957), Vol. 5.

The Zeeman interaction between two states m and n is given[10] by

$$H_{mn}{}^Z=\mu_B\mathbf{H}\cdot\sum_{i=1}^{6}\alpha_m{}^i\alpha_n{}^i[g_l\mathbf{I}+(g_l-g_t)\mathbf{U}^i]\cdot\mathbf{S}, \qquad (9)$$

where the α^i are the coefficients in the wave function, $\mathbf{I}$ is the unit tensor, and $\mathbf{U}^i$ is a tensor which selects the ith valley along one of the [100] axes. Using the orthogonality condition

$$\sum_{i=1}^{6}\alpha_m{}^i\alpha_n{}^i=\delta_{mn},$$

we obtain

$$H_{mn}{}^z=\mu_B\mathbf{H}\cdot[g_t\delta_{mn}+(g_l-g_t)\mathbf{D}_{mn}]\cdot\mathbf{S},$$

where

$$\mathbf{D}_{mn}=\sum_{i=1}^{6}\alpha_m{}^i\alpha_n{}^i\mathbf{U}^i. \qquad (10)$$

Because $g_l-g_t\simeq 0.001$,[7] the off-diagonal Zeeman interaction matrix elements are small, however it is just these off-diagonal Zeeman terms which couple to 1S doublet states [(10) will not connect the 1S singlet and triplet states] which Hasegawa[10] and Roth[11] use to successfully explain the low-temperature single-phonon T_s process. The ground-state singlet Zeeman interaction is isotropic with a g value, $g_0=1/3(g_l+2g_t)$, but all the other 1S states have anisotropic g values and can contribute to the spin-lattice relaxation.

The hyperfine interaction with the donor nucleus results from the Fermi contact term. For the ground-state singlet the hyperfine interaction is given by $(8\pi/3)g\mu_B g_n\mu_{Bn}|\psi_0(0)|^2$, while for all the other 1S states the hyperfine interaction is zero. Similarly, there are no hyperfine interaction matrix elements between the ground state and any of the 1S excited states.

B. The Orbit-Lattice Interaction

For the calculations we employ the familiar deformation potential approach,[33] using specificially the deformation potential for many-valley semiconductors[34] containing a pure dilatational deformation potential Ξ_d, and a pure shear deformation potential Ξ_u. The deformation potential change due to a phonon of wave number $\mathbf{q}$ and polarization $\mathbf{e}_s(\mathbf{q})$ is $\frac{1}{2}[\delta E_k(\mathbf{e}_s,\mathbf{q})+\delta E_{k'}\times(\mathbf{e}_s,\mathbf{q})]$ where $\mathbf{k}$ is the initial electron wave vector and $\mathbf{k}'$ the final wave vector after interaction with the phonon. The atom displacement, $\mathbf{Q}(\mathbf{r})$, due to acoustic modes only, is given by

$$\mathbf{Q}(r)=\sum_{\mathbf{q},s}[\mathbf{e}_s(\mathbf{q})a_q e^{i\mathbf{q}\cdot\mathbf{r}}+e_s{}^*(\mathbf{q})a_q{}^*e^{-i\mathbf{q}\cdot\mathbf{r}}]. \qquad (11)$$

The amplitudes a_q and $a_q{}^*$ are phonon operators with

[33] J. Bardeen and W. Shockley, Phys. Rev. **80**, 72 (1950).
[34] C. Herring and E. Vogt, Phys. Rev. **101**, 944 (1956).

matrix elements

$$(n_q-1\,|\,a_q\,|\,n_q)=[\hbar n_q/2M_c\omega_q]^{1/2},$$
$$(n_q+1\,|\,a_q^*\,|\,n_q)=[\hbar(n_q+1)/2M_c\omega_q]^{1/2}, \quad (12)$$

where M_c is the mass of the crystal and n_q $[n_q=1/\times(e^{\hbar\omega q/kT}-1)]$ is the phonon occupation number of the mode with wave number $\mathbf{q}$. The Fourier component of the energy shift due to the $\mathbf{q}$th mode with polarization $\mathbf{e}_s$ is given by

$$\delta E_{q,s}=\{\Xi_d(\mathbf{e}_s\cdot\mathbf{q})+\tfrac{1}{2}\Xi_u[(\mathbf{q}\cdot\mathbf{K}_i)(\mathbf{e}_s\cdot\mathbf{K}_i)+(\mathbf{q}\cdot\mathbf{K}_j)(\mathbf{e}_s\cdot\mathbf{K}_j)]\}a_q e^{i\mathbf{q}\cdot\mathbf{r}}+\text{c.c.}, \quad (13)$$

where $\mathbf{K}_i$ and $\mathbf{K}_j$ are unit vectors to the ith and jth valleys, replacing $\mathbf{k}$ and $\mathbf{k}'$. At this juncture only two types of transitions ($\mathbf{k}\rightarrow\mathbf{k}'$) are considered, intravalley scattering with $\mathbf{K}_i=\mathbf{K}_j$ and intervalley scattering (to opposite valley only) Umklapp processes with $\mathbf{K}_i=-\mathbf{K}_j$. The matrix element for the absorption of a phonon by the donor will be $H_{mn}^{\text{o1}}=\int\psi_m^*(\delta E_{q,s})\psi_n dV$ given by

$$\sum_{i,j}\alpha_m{}^i\alpha_n{}^j[\Xi_d(\mathbf{e}_s\cdot\mathbf{q})+\Xi_u(\mathbf{q}\cdot\mathbf{K}_i)(\mathbf{e}_s\cdot\mathbf{K}_i)]\times a_q\int F_i^*F_j u_{k_i}^* u_{k_j}e^{+i(\mathbf{q}+\mathbf{k}_j-\mathbf{k}_i)\cdot\mathbf{r}}dV. \quad (14)$$

We have restricted ourselves to terms with $F_i=F_j$ and $u_{k_i}=u_{k_j}$. Expanding the periodic $u_k^*u_k$ in terms of reciprocal lattice vectors, the integral in (14) becomes

$$\sum_\nu C_{k_i}{}^\nu\int|F_i|^2e^{i(\mathbf{k}_j+\mathbf{q}-\mathbf{k}_i+\mathbf{K}_\nu)\cdot\mathbf{r}}d\mathbf{r}. \quad (15)$$

The hydrogenic $|F_i|^2$ may be Fourier analyzed using

$$|F_i|^2=\frac{1}{(2\pi)^3}\sum f(\lambda_i)\exp(-i\lambda_i\cdot\mathbf{r}), \quad (16)$$

which then reduces the integral in (15) to a δ function. The result for H_{mn}^{o1} is

$$H_{mn}^{\text{o1}}=\sum_{i,j}\alpha_m{}^i\alpha_n{}^j[\Xi_d(\mathbf{e}_s\cdot\mathbf{q})+\Xi_u(\mathbf{q}\cdot\mathbf{K}_i)(\mathbf{e}_s\cdot\mathbf{K}_i)]\times a_q\sum_\nu C_{k_i}{}^\nu f^{ij}(\mathbf{K}_\nu+\mathbf{q}+\mathbf{k}_j-\mathbf{k}_i). \quad (17)$$

For the $i=j$ intravalley terms $\mathbf{k}_i=\mathbf{k}_i$ and the only large term is the $\mathbf{K}_\nu=0$ term. In this case we have just Hasegawa's result,[10] namely,

$$H_{mn}^{\text{o1}}(i=j)=[\Xi_d q_l f(\mathbf{q}_l)\delta_{mn}+\Xi_u\sum_{i=j}^{6}\alpha_m{}^i\alpha_n{}^i\times(\mathbf{q}\cdot\mathbf{K}_i)(\mathbf{e}_s\cdot\mathbf{K}_i)f^i(\mathbf{q})]a_q, \quad (18)$$

whereas for the Umklapp process $i\neq j$ case ($\mathbf{k}_j=-\mathbf{k}^i$)

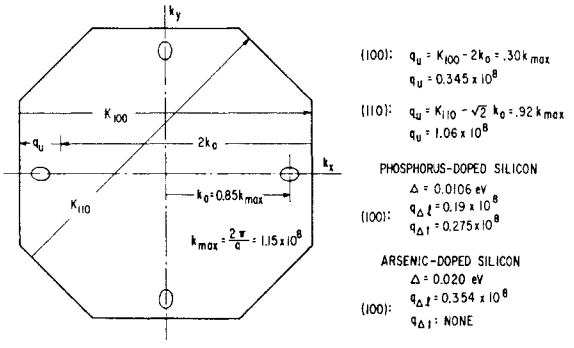

FIG. 16. A (001) plane cross section of the first Brillouin zone for Si showing the conduction band minima and possible Umklapp-type intervalley H^{o1} matrix elements. Only the intervalley process from a given valley to the opposite valley has a small enough required umklapp vector $\mathbf{q}_u$ to be important. The resonant longitudinal and transverse wave numbers q_Δ are listed for both P and As. The As $q_{\Delta l}$ is very close to the required q_u for opposite valley intervalley Umklapp.

the matrix element becomes

$$H_{mn}^{\text{o1}}(i\neq j)=\sum_{i\neq j}{}'\alpha_m{}^i\alpha_n{}^j[\Xi_d q_l a_q+\Xi_u(\mathbf{e}_s\cdot\mathbf{K}_i)(\mathbf{q}\cdot\mathbf{K}_i)a_q]\times\sum_\nu C_{k_i}{}^\nu f^i(\mathbf{K}_\nu+\mathbf{q}-2\mathbf{k}_i). \quad (19)$$

The only important Umklapp terms are for the six smallest reciprocal lattice vectors along the [100] axis. The f^i decrease very rapidly for large arguments. The matrix element will only be large for values of $\mathbf{q}\simeq2\mathbf{k}_i-\mathbf{K}_\nu$. Since $|k_i|=0.85k_{\max}$ ($k_{\max}=q_{\max}$), we can define an Umklapp phonon wave number $\mathbf{q}_{u_i}=(2\mathbf{k}_i-\mathbf{K}_i)$ with the magnitude $|q_u|=0.30q_{\max}$. Figure 16 shows a (001) plane cross section of the first Brillouin zone illustrating the various Umklapp processes.

A typical matrix element between the 1S singlet and a 1S triplet will be

$$H_{03}^{\text{o1}}=(1/2\sqrt{3})[\Xi_d q_l+\Xi_u e_x q_x]a_q\times C_{k_0}{}^1[f^x(-q_u\hat{x}+\mathbf{q})-f^x(q_u\hat{x}+\mathbf{q})], \quad (20)$$

where $\hat{x}$ is a unit vector in the x direction. The two terms do not cancel for large enough values of q_u and H_{03}^{o1} will peak for values of $\mathbf{q}=\pm q_u\hat{x}$. Although the intravalley H^{o1} terms connect the 1S singlet to the 1S doublet only, the intervalley Umklapp terms connect the 1S singlet to both the 1S doublet and triplet. Calculation of the "resonance phonon" q_Δ's ($q_\Delta=\Delta/\hbar v$) where Δ is the measured valley-orbit splitting indicates the q_Δ's are in the range where Umklapp will be important (see Fig. 16). For the arsenic donor q_Δ is very close to $0.30q_{\max}$, the value needed to maximize f. For arsenic the intervalley H^{o1} should be much more important than the intravalley H^{o1} for phonons with $\mathbf{q}$ close to q_Δ. Since H^{o1} is proportional to f we may use the magnitude of f as a measure of the strength of the orbit-lattice interaction. Following Hasegawa,[10] the f function is the inverse Fourier

TABLE III. Relative strength of the orbit-lattice interaction for intravalley processes $[H^{ol} \propto f(\tilde{q}_\Delta)]$ and intervalley processes $[H^{ol} \propto f^x(\mathbf{q}_\Delta - q_u\hat{x})]$ in the short-wavelength region for resonant phonons ($q_\Delta = \Delta/\hbar v$). $\tilde{q}_\Delta$ represents an effective wave number using an effective sound velocity averaged over solid angle. $q_{\Delta[100]}$ is the wave number for a phonon propagating along a [100] axis. For Si, $a^* = 20\times10^{-8}$ cm.

Donor	Mode	$\tilde{q}_\Delta$ (10^8 cm^{-1})	$\tilde{q}_\Delta a^*$	$f(\tilde{q}_\Delta)$	$q_{\Delta[100]}$ (10^8 cm^{-1})	$f_{\max}{}^x(\mathbf{q}_\Delta - q_{ux}\hat{x})$ $q_x = q_\Delta$, $q_y = q_z = 0$
P	long.	0.173	2.45	0.063	0.190	0.20
	trans.	0.297	5.94	0.010	0.274	0.63
As	long.	0.323	6.45	0.0077	0.354	0.99
	trans.	none	···	0	···	0
Bi	long.	0.554	10.97	0.0010	0.608	0.049
	trans.	none	···	0	···	0

transform of (16). For the two cases one has

$$\text{Intravalley } f^x(\mathbf{q}) = 1/\{1+\tfrac{1}{4}[q_x{}^2b^2+(q_y{}^2+q_z{}^2)a^2]\}^2, \quad (21)$$

$$\text{Intervalley } f^x(-q_{ux}\hat{x}+\mathbf{q}) = 1/\{1+\tfrac{1}{4}[(q_x-q_u)^2b^2+(q_y{}^2+q_z{}^2)a^2]\}^2.$$

For the resonant phonons $q_\Delta b > 1$ and the long-wavelength approximation ($f \sim 1$) is poor. Table III shows typical f values in the short-wavelength region for intravalley and intervalley processes. It should be noted that $f^x(\mathbf{q}-q_u\hat{x})$ is strongly peaked along the x axis when q_Δ is close to q_u. Table III only indicates the maximum value of $f^x(\mathbf{q}_\Delta - q_u\hat{x})$. When $|f^x|^2$ is averaged over solid angles this will be reduced somewhat. In fact, for P the effect of intravalley and intervalley H^{ol} on the spin-lattice relaxation rate are comparable. However, for As, and Bi to a lesser extent, the intervalley Umklapp processes will be dominant. For As and Bi, Δ is large enough to exclude transverse acoustical phonons. Even for P, longitudinal phonons have assumed a greater importance in the short-wavelength region than in the long-wavelength region. This is because, although the density of longitudinal modes per unit frequency is much less than for transverse modes, the interference is much less for longitudinal phonons of a given energy than for transverse phonons of the same energy.

To obtain relaxation rates one must evaluate quantities like $\int |H_{mn}{}^{ol}(q) H_{pr}{}^{ol}(q)|\, d\Omega_q$, representing the average over solid angle of the absorption $|H^{ol}|^2$ matrix element squared. This is done in the Appendix. In calculating the orbit-lattice interaction the deformation-potential constants Ξ_d and Ξ_u have been assumed to be independent of q and equal to the long-wavelength values. For such high-q phonons near $q_{\max}$, the deformation potential constants might be substantially different than the long-wavelength values.

C. The Raman T_s-Power Law Region

Roth[11] has evaluated the Raman spin-lattice relaxation rate $1/T_s$ using the valley repopulation g-value anisotropy spin-flip mechanism which involves only the $1S$ doublet states. This calculation is briefly sketched here. The matrix element for a spin flip of a donor electron in the ground state is

$$(0'|M|0) = \sum_{k,j} \frac{H_{0'j}H_{jk}H_{k0}}{(E_0-E_j)(E_0-E_k)}, \quad (22)$$

where $0 = |0,1/2,n_q,n_{q'}\rangle$ and $0' = |0,-1/2,n_q-1,n_{q'}+1\rangle$.

At sufficiently low temperatures the Raman relaxation is due to thermal phonons ($\hbar\omega \sim kT$). The long-wavelength approximation is valid [$qa \ll 1$, $f(\mathbf{q}) \sim 1$], furthermore longitudinal phonons can be neglected because of their low density of states compared with transverse phonons. The $1S$ triplet states can be neglected and the sum in (22) is over orbital states 1 and 2. Twenty-four terms remain in (22) with several different energy denominators which become identical when the phonon energy and Zeeman energy are negligible compared with Δ. $|(0'|M|0)|^2$ is then averaged over solid angle for the incoming phonon, $\mathbf{q}$, and the outgoing phonon, $\mathbf{q}'$. The various matrix elements and solid angle averages of $\langle|H_{ij}{}^{ol}H_{kl}{}^{ol}|\rangle_{\Omega q}$ are tabulated in the Appendix. After some algebra one has

$$|(0'|M|0)|^2 = \frac{2(g_l-g_t)^2(\mu_B H)^2 f(\theta,\phi)}{\Delta^4} \times \langle|H_{02}{}^{ol}(\mathbf{q})|^2\rangle_{\Omega q}\langle|H_{02}{}^{ol}(q')|^2\rangle_{\Omega q'}, \quad (23)$$

where $f(\theta,\phi)$ is Hasegawa's angular function.[10] Using (8), (12), and (A5) the transition probability (neglecting the longitudinal lattice modes) becomes

$$W_{0'\leftarrow 0} = \frac{2}{225(2\pi)^3}\left(\frac{\Xi_u}{\Delta}\right)^4 (C_{k_0}{}^0)^4 \frac{(g_l-g_t)^2(\mu_B H)^2 f(\theta,\phi)}{\rho^2} \times \int_0^{q_{max}} [qf^2(q)n_q][q'f^2(q')(n_{q'}+1)]q^2q'^2dq. \quad (24)$$

We set $q' = q$ and $C_{k_0}{}^0 \simeq 1$. We use $\omega = q\bar{v}_t$ and make the substitution $\hbar\omega/kT = x$. Now (24) becomes

$$W_{0'\leftarrow 0} = \frac{2}{225(2\pi)^3}\left(\frac{\Xi_u}{\Delta}\right)^4 \frac{(g_l-g_t)^2(\mu_B H)^2 f(\theta,\phi)}{\rho^2\bar{v}_t{}^{10}} \times \left(\frac{kT}{\hbar}\right)^7 \int_0^{\theta_{D/T}} \frac{x^6e^x dx}{(e^x-1)^2}. \quad (25)$$

For $T \ll \theta_{Dt}$, the integral is nearly 6!. The final result for $1/T_s$ ($1/T_s = W_{0'\leftarrow 0} + W_{0\leftarrow 0'} \simeq 2W$) is

$$\frac{1}{T_s} = \frac{8}{5\pi^3}\left(\frac{\Xi_u}{\Delta}\right)^4 \frac{(g_l-g_t)^2(\mu_B H)^2 f(\theta,\phi)}{\rho^2\bar{v}_t{}^{10}}\left(\frac{kT}{\hbar}\right)^7. \quad (26)$$

This result is slightly smaller than Roth's Raman calculation.[11] Using Wilson and Feher's values[7] of $\Xi_u/\Delta = 0.76\times10^3$, $g_l - g_t = 1.04\times10^{-3}$ and also $\rho = 2.33$, $\bar{v}_t = 5.42\times10^5$, and $H = 3200$ G one obtains $T_s \sim 5.0\times10^4$

sec at 4.2°K in contrast with the experimental value of 25 sec. Furthermore, the experimental results show no field dependence between 3000 and 8000 G[7] and no angular dependence at 4.2°K within experimental error. Taking the ratio of T_s (direct) to T_s(Raman) for the Hasegawa-Roth mechanism one obtains

$$\frac{T_s(\text{direct})}{T_s(\text{Raman})}=\frac{27}{\pi^2}\left(\frac{\Xi_u}{\Delta}\right)^2\frac{(kT)^6}{\rho\bar{v}_t^5\hbar^3(\mu_B H)^2}. \tag{28}$$

Using the above numbers the two processes would be competitive at 4.8°K, whereas the experimental results of Feher and Honig indicate a change to the Raman process near 2.5°K. The experiments and calculations suggest another mechanism. Roth[35] has calculated another process contributing to T_s(direct) which arises from a phonon modulation of the g shift within a single valley. Wilson and Feher[7] have shown that the two mechanisms of g modulation give excellent agreement of the angular dependence and the magnitude of T_s at 1.25°K. However, this second mechanism used for a Raman process would yield an H^2T^7 dependence which is contrary to experiment.

The H^0T^9 dependence of the Raman $1/T_s$ points to the spin-orbit interaction, H^{so}, as the spin-flip H^{nd}. However, tetrahedral symmetry only permits nonzero $H_{mn}{}^{so}$ among the $1S$ triplet states and also between the $1S$ doublet and triplet states. The magnitudes of such $H_{mn}{}^{so}$ are unknown, moreover at least one of the H^{ol}'s will have to be $H_{m0}{}^{ol}$, $m=3$, 4, or 5. For $qa\ll 1$, $|H_{30}{}^{ol}|^2$ will be small because of the cancellation of

$$[f^x(\mathbf{q}+q_u\hat{x})-f^x(\mathbf{q}-q_u\hat{x})].$$

Furthermore, $|H_{30}{}^{ol}|^2\propto a_q{}^2q^4$ rather than $a_q{}^2q^2$ for the intravalley matrix elements. This would then lead to a T^{11} temperature dependence for $1/T_s$. The coefficient would be small.

Another possibility is a process involving H^{so} and H^{ol} matrix elements to other bands. Liu[36] has examined spin-orbit effects and the g values for the Si conduction band. Recently, Roth and Ham[37] have independently calculated an isotropic, field-independent T^9 process using only conduction band (Δ_1) and valence band (Δ_5) states. Ham's result is

$$\frac{1}{T_s}=\frac{3584}{5\pi^3}\frac{(kT)^9}{\rho^2\hbar^7\bar{v}_t{}^{10}}\times\left[\left(\frac{\Xi_u}{\Delta}\right)\left(\frac{(\Delta_{5y}|h_x|\Delta_1)(\Delta_1|E_{yz}|\Delta_{5y})}{E_{15}{}^2}\right)\right]^2, \tag{28}$$

where $(\Delta_{5y}|h_x|\Delta_1)$ has been calculated by Liu,[36] $(\Delta_1|E_{yz}|\Delta_{5y})$ is an interband matrix element of the deformation potential, and E_{15} is the energy difference between Δ_1 and Δ_5. Using a reasonable guess for $(\Delta_1|E_{yz}|\Delta_{5y})$ and Liu's value for $(\Delta_{5y}|h_x|\Delta_1)$, one finds (28) to be about two orders of magnitude too weak although it has all the correct qualitative features. Equation (28) shows $T_s\propto\Delta^2$, roughly consistent with the C constants for P and As in Table II. Nevertheless, the origin of the power-law Raman T_s must be considered in doubt.[37a]

D. Resonant Exponential Relaxation

Because $k\theta_D>\Delta$ there are phonons with energy $\hbar\omega$ near Δ which are very effective relaxers because of a resonant absorption-emission process. This case has been treated by Orbach[16] for rare-earth ions in crystals in which the low-lying levels are spin levels and $S\geq 1$. $S=1/2$ for the shallow donors in silicon, hence the exponential relaxation involves different orbital levels. The resonant process is a three-step process in the following sequence. First, a phonon of energy $\hbar\omega\simeq\Delta$ is absorbed, putting the donor electron into one of the $1S$ doublet or triplet states. While in this state there is a small probability the spin will be flipped before the donor electron decays to the ground state with the spontaneous emission of a phonon.

If we consider the matrix element $M_{0'\leftarrow 0}$ in (22) the following types of energy denominators occur in the sum (emission first, then absorption will not produce resonant denominators).

(A) Spin flipping term first or last

$$\times\frac{1}{(\Delta-\hbar\omega)(\Delta-g\mu_B H)}, \tag{29}$$

(B) Spin flipping term in middle

$$\times\frac{1}{(\Delta-\hbar\omega)(\Delta+g\mu_B H-\hbar\omega)}.$$

In calculating $W_{0'\leftarrow 0}$, (29) will enter squared, hence the integral over phonon energy will involve a second-order pole for term A and two second-order poles, separated in energy by $g\mu_B H$, for term B. The integration over phonon energy in $W_{0'\leftarrow 0}$ diverges because of the second-order poles. Following Orbach,[16] a level width for the excited states is introduced, as is done for the resonance fluorescence of photons in gases and for resonant nuclear absorption phenomena. The level width Γ may be due to spontaneous emission of a phonon or photon, or might be due to strain. The level width is considered in

[35] L. Roth, Massachusetts Institute of Technology, Lincoln Laboratory Reports, 1960 (unpublished).

[36] L. Liu, Phys. Rev. **126**, 1317 (1962).

[37] (Private communication.) The author is grateful to F. Ham for considering the question of a field-independent T^9 process. This process was suggested by the experimental results and Van Vleck's pioneering work (see reference 17). We have learned that L. Roth has also calculated this process and obtains a similar result.

[37a] *Note added in proof.* The author has recently learned that L. Roth and H. Hasegawa and M. Nakayama have calculated a new T^9 mechanism based on the breakdown of the effective mass approximation. They use the impurity potential to admix the Δ_2' band, thus going to one order higher perturbation theory. Surprisingly, the result is one to two orders of magnitude more effective than (28) and would be close to the experimental result.

Sec. VII. For the B term an integral of the following form arises:

$$\int_0^{\omega max} \frac{G(\omega)d\omega}{[(\Delta-\hbar\omega)^2+(\Gamma/2)^2][(\Delta+g\mu_BH-\hbar\omega)^2+(\Gamma/2)^2]}. \tag{30}$$

The function $G(\omega)$, which may be a complicated function of ω, is, nevertheless, slowly varying in the region of resonance compared to the energy denominator ($\Gamma\ll\Delta$) and may be removed from the integral. The integral is, then, readily evaluated for two distinct cases, $g\mu_BH\ll\Gamma$ and $g\mu_BH\gg\Gamma$. The result is

$$\frac{4\pi}{\hbar}G\left(\frac{\Delta}{\hbar}\right)\times\begin{matrix}1/\Gamma^3, & g\mu_BH\ll\Gamma,\\ 1/\Gamma[(g\mu_BH)^2+(\Gamma/2)^2], & g\mu_BH\gg\Gamma.\end{matrix} \tag{31}$$

It is noted for $g\mu_BH\ll\Gamma$ the two second-order poles are not resolved and the integrand behaves as if it contains a fourth-order pole. It is also easy to show that the integral of the A term is smaller than the B term by $(\Gamma/\Delta)^2$ or $(g\mu_BH/\Delta)^2$. These are both very small quantities. The most effective resonant relaxation comes from exciting the electron to the $1S$ doublet and triplet states and letting it relax while there. The process might be considered "excited state spin-lattice relaxation."

$W_{0'\leftarrow 0}$ can be divided into three types of terms, W^N intravalley and W^U intervalley terms, where the N and U refer to the normal and Umklapp orbit-lattice interactions, and mixed terms W^{NU}. It can be shown that $\int H_{0m}{}^{01}H_{0n}{}^{01}d\Omega_q\propto\delta_{mn}$, hence all cross terms in the matrix element $|(0'|M|0)|^2$ are zero. The W^N terms result from states 1 and 2 only, while the W^U arises from all the states 1–5. If H^{sf}, the spin-flip interaction, doesn't connect the doublet and triplet, then the mixed terms could occur only within the doublet. For simplicity the mixed terms will be neglected.

(1) *The Intravalley Relaxation Rate* W^N

Using (8), (12), (A6), and (31), the result for W^N will be

$$W_{-1/2\leftarrow 1/2}{}^N=\frac{2}{\hbar}\left\{\frac{\Xi_u{}^2}{36\pi\rho}\left(\frac{\Delta}{\hbar}\right)^3\left[\frac{6}{5}\frac{f^2(\bar{q}_{\Delta l})}{\bar{v}_l{}^5}+\frac{4}{5}\frac{f^2(\bar{q}_{\Delta l})}{\bar{v}_l{}^5}\right]\times\frac{e^{\Delta/kT}}{(e^{\Delta/kT}-1)}\right\}^2 e^{-\Delta/kT}\left(\sum_{1,2}|H_{ij}{}^{sf}|^2\right)\times\begin{matrix}1/\Gamma^3, & g\mu_BH\ll\Gamma\\ 1/\Gamma[(g\mu_BH)^2+(\Gamma/2)^2, & g\mu_BH\gg\Gamma.\end{matrix} \tag{32}$$

It is written in this form because the quantity in the braces is just the minimum level width $\Gamma^N=\hbar W^{sp}$, where W^{sp} is the transition probability for spontaneous intravalley phonon emission. Hence, the spin-lattice relaxation takes the particularly simple form

$$W_{-1/2\leftarrow 1/2}{}^N=2\left(\frac{\Gamma^N e^{-\Delta/kT}}{\hbar}\right)\times\left[\frac{\sum_{1,2}|H_{ij}{}^{sf}|^2}{(g\mu_BH)^2+(\Gamma/2)^2}\right],\qquad \Gamma^N\ll g\mu_BH. \tag{33}$$

The factor $W^{sp}e^{-\Delta/kT}$ is the transition probability for exciting a donor electron to one of the doublet states by the absorption of a phonon of energy $\hbar\omega\sim\Delta$ (both doublet states have the same Γ^N). The second factor represents the effectiveness of the doublet spin-relaxing mechanisms by measuring them relative to the Zeeman energy. For the Hasegawa-Roth mechanism the second factor would be of order $(4/9)(g_l-g_t)^2/g^2$ for small Γ. The 4 arises from the number of cross paths of H^{sf} between states 1 and 2. The 2 in front in (33) results from the integration in (30) and represents the equivalence of a process with absorption and emission energies Δ and $\Delta-g\mu_BH$, respectively, with a second process with absorption and emission energies $\Delta+g\mu_BH$ and Δ, respectively.

The particular Γ dependence of (33) is not present in Orbach's result.[16] Orbach's second-order perturbation calculation involved spin flips between the ground state and the excited state. Here, in third-order perturbation theory, the spin is predominately flipped between the different excited states. When the donor electron is in the excited states for a time τ such that $\tau\omega_{\text{larmor}}>1$ H^{sf} can be fully effective, however, as the lifetime in the excited states decreases until it is less than the Larmor period ($\Gamma/2>g\mu_BH$) H^{sf} becomes less effective and W^N starts to fall off as $1/\Gamma$. W^N is maximum for $\Gamma=2g\mu_BH$.

If numbers are inserted in (33), namely, $\Gamma/\hbar=4\pi\times10^{10}$ sec^{-1} and $g_l-g_t\simeq10^{-3}$, the Hasegawa-Roth mechanism gives $1/T_s\simeq2.8\times10^4\,e^{-\Delta/kT}$ in contrast to an experimental value of $1/T_s\simeq2.2\times10^8\,e^{-\Delta/kT}$ for P. This disagreement by a factor of 8 000 is slightly larger than that for the T^7 Raman T_s calculation suggesting that the same unknown mechanism may be accounting for the much faster relaxation for the power law and the exponential temperature ranges.

(2) *The Intervalley Relaxation Rate* W^U

For pure intervalley spin-lattice relaxation the result will be the same as (33) except that we replace Γ^N with Γ^U and the sum of $H_{ij}{}^{sf}$ is over all excited states 1 to 5. $\Gamma^U=2\pi|H_{m0}{}^{01}|^2\rho_{Ef}$ and using (A7) we have

$$\Gamma^U=\frac{(C_{k_0}{}^1)^2}{24\pi\rho}\left(\frac{\Delta}{\hbar}\right)^3\left\{\frac{\Xi_u{}^2I_l{}^4}{v_{l[100]}{}^5}\right]1+2\frac{\Xi_dI_l{}^2}{\Xi_uI_l{}^4}+\left(\frac{\Xi_d}{\Xi_u}\right)^2\frac{I_l{}^0}{I_l{}^4}\Big]+\frac{\Xi_u{}^2(I_l{}^2-I_t{}^4)}{v_{t[100]}{}^5}\Big\}, \tag{34}$$

where the I^n are given in the Appendix. $v_{l[100]}$ and $v_{t[100]}$ are used rather than mean values because the $|H_{m0}^{01}|^2$ are only large along the [100] axis. $C_{k_0}{}^1$ is not known but a crude estimate places it in the range 0.3 to 0.7. The real difficulty with (34) is the lack of knowledge of Ξ_d. Hydrostatic pressure experiments[38] help determine $E_{1c}-E_{1v}$, the difference in dilatational energies of the conduction and valence bands ($E_{1c}=\Xi_d+\frac{1}{3}\Xi_u$). However, E_{1c} and E_{1v} are not readily separated. If Ξ_d were negative and close to the Ge value of -6.9 eV, the longitudinal term in (34) would nearly cancel. We consider the longitudinal part as including an unknown parameter σ (inside brackets) which might reasonably lie within the limits 0.1 and 4.

For P both longitudinal and transverse phonons contribute to (34) and Γ^N may be slightly larger than Γ^U depending on $C_{k_0}{}^1$ and Ξ_d. For As with $C_{k_0}{}^1\sim 0.5$, $(\Gamma^U/\Gamma^N)\sim 100$ for $\Xi_d=0$. It would be fortuitous if Ξ_d were such to reduce Γ^U/Γ^N to less than 10% of the above value. Hence, for As it would appear that $\Gamma^U\gg\Gamma^N$. It is also likely that $\Gamma(\text{As})\geq\Gamma(\text{P})$. We calculate $W^{sp}(1S$ doublet$)>2.5\times10^{10}$ sec^{-1} and $W^{sp}(1S$ triplet$)>0.6\times10^{10}$ sec^{-1} for P donors. The P values of Γ are at least within a factor of 5 of the value which maximizes (33). It would appear that the large experimental $E(\text{As})/E(\text{P})$ ratio would have to be explained almost entirely by a large ratio $H^{sf}(\text{As})/H^{sf}(\text{P})$. The still larger E constants for Sb and Bi, suggest successively larger H^{sf}'s for Sb and Bi. This conclusion, if correct, disagrees with effective mass theory and would lend support to an atomic-type impurity spin-orbit H^{sf}. A relaxation process involving interband matrix elements might remove this difficulty.

E. The Raman T_x Process (Long-Wavelength Region)

Wilson and Feher[7] have discussed the T_x process noting that the Pines, Bardeen, Slichter calculation[8] of $1/T_x$ greatly overestimated the amplifying effect of a dilation on $\delta|\psi_0(0)|^2$. Hasegawa[7,39] has calculated a Raman $1/T_x$ depending on the modulation of the hyperfine interaction by the phonon-induced admixture of the $1S$ doublet states, this admixture reducing the hyperfine interaction ($1S$ doublet and triplet states have no contact hyperfine interaction). Hasegawa also demonstrated for a strain-free crystal that this process does not permit a single phonon $1/T_x$. This mechanism can be calculated by treating H^{01} as a perturbation, obtaining the perturbed wave functions to second order, then calculating the hyperfine interaction between states $|0,1/2,m_I,n_q,n_{q'})$ and $|0,-1/2,m_I+1,n_q-1,n_{q'}+1)$. The result for W_x is

$$W_{xM_I}=\frac{2\pi}{\hbar}A^2|(-\tfrac{1}{2},M_I+1|\mathbf{I}\cdot\mathbf{S}|\tfrac{1}{2},M_I)|^2\times\sum_n\frac{\langle|H_{0n}^{*01}|^2\rangle_{\Omega_{q'}}\langle|H_{n0}^{01}|^2\rangle_{\Omega_q}}{(-\hbar\omega'-\Delta)^2(\hbar\omega-\Delta)^2}\rho_E, \quad (35)$$

where the sum is restricted to the $1S$ doublet states for the long-wavelength region. $A=(8\pi/3)(g\mu_B g_n\mu_{Bn})\times|\psi_0(0)|^2$, the magnitude of the hyperfine interaction. Inserting (A5), the density of states for the more dense transverse modes, and integrating over frequency one obtains Hasegawa's final result for $T_x(m_I=I-1)$ is

$$\frac{1}{T_x}=\frac{8}{5\pi^3}\frac{A^2I}{\rho^2\bar{v}_t^{10}}\left(\frac{\Xi_u}{\Delta}\right)^4\left(\frac{kT}{\hbar}\right)^7. \quad (36)$$

Comparing this result with that for the T^7 Raman T_s using the Hasegawa-Roth mechanism, one obtains the ratio

$$\frac{T_s}{T_x}=I\frac{g^2}{(g_l-g_t)^2}\left(\frac{\Delta H_{hf}}{H}\right)^2, \quad (37)$$

where ΔH_{hf} is the hyperfine splitting of the donor electron. This ratio for P with $\Delta H_{hf}=42$ G, $g_l-g_t\simeq 0.001$, and $H=3300$ G is about 300, whereas the experimental ratio is about 0.2 in the Raman temperature range. For As the disagreement is even worse.

Table IV compares calculated values of T_x with experimental values. The agreement of the experimental and calculated values using (36) is surprisingly good except for Sb^{121}. However, the measured T_x in sample C is only approximate and at 2.2°K it is possible one is in the linear temperature-dependent range which would result from internal strains. The significant result is the agreement with $1/T_x\propto(\Delta H_{hf})^2I/\Delta^4$. The longer T_x for As than for P and the surprisingly long value of T_x for Bi must be attributed to the significantly greater Δ values for As and Bi. The phonon modulation of the hyperfine interaction via the $1S$ doublet states satisfactorily accounts for the T_x Raman process in the long-wavelength region. This is in sharp contrast to the disagreement for the Raman T_s as emphasized by (37).

TABLE IV. Comparison of calculated and experimental T_x's.

Donor	I	ΔH_{hf} (g)	Δ (eV$\times10^{-3}$)	T (°K)	T_x(calc) (sec)	T_x(expt) (sec)
P^{31}	1/2	42	10.6	2.16	16 000	11 000 (reference 6)
				(4.2)	(150)	(105)
As^{75}	3/2	71	19.8	4.2	210	160
Sb^{121}	5/2	67	9.1	2.2	600	100
Bi^{209}	9/2	528	34	4.2	11.2	7

F. T_x Process—Resonant Exponential Temperature-Dependent Case

The hyperfine spin-lattice relaxation process responsible for T_x can have a resonant absorption-emission

[38] W. Paul, J. Phys. Chem. Solids 8, 196 (1959); J. Appl. Phys. 32, 2082 (1961).

[39] (Private communication.) The author also independently calculated this process for $1/T_x$, but is grateful to H. Hasegawa for communicating his results to the author and for pointing out a numerical mistake in the author's calculation.

process involving phonons with energy $\hbar\omega\sim\Delta$. Equation (35) shows a single second-order pole at $\hbar\omega=\Delta$. Following the same procedure used for the T_s exponential relaxation case it is straightforwardly shown that

$$\frac{1}{T_x}=\left(\sum_n \frac{\Gamma_n e^{-\Delta/kT}}{\hbar}\right)\left(\frac{A}{\Delta}\right)^2 I, \tag{38}$$

where the first term represents the total absorption probability to all the $1S$ valley-orbit states, each having a level width Γ_n associated with a phonon spontaneous emission rate $W_n{}^{sp}$. However, this process is very weak. Inserting numbers for P, namely, $(A/\Delta)^2\simeq 2.0\times10^{-9}$ and $\sum_n \Gamma_n/\hbar\simeq10^{11}$ sec^{-1}, yields a T_x of 4 sec at 20.4°K, many orders of magnitude longer than the extrapolated T^7 process T_x at 20°K. The exponential temperature-dependent T_x will never catch up to the T^7 process as the temperature is increased, unless the T^7 term is strongly reduced due to the breakdown of the long-wavelength approximation at high temperature. If T_x were to have an exponential temperature dependence, it would begin at a temperature well above where T_s starts to exhibit an exponential temperature dependence.

G. Summary of Calculations and Comparison with Experiment

The measured power-law Raman T_s is three orders of magnitude shorter than the calculated T_s based on the Hasegawa-Roth mechanism. So far it has not been possible to show how the spin-orbit interaction, a likely candidate for the spin-flipping mechanism, might explain the experimental results.[37a] The measured exponential temperature-dependent T_s is also nearly four orders of magnitude shorter than the calculated value if the Hasegawa-Roth mechanism is used. Here, the calculated $1/T_s$ exhibits a maximum relaxation rate when the excited-state lifetime is equal to the Larmor period, a result of the dominance of the terms involving a spin-flip interaction as the middle term. Here also the results suggest that the spin-flip matrix element must get larger for the heavier donor impurity atoms.

The calculated Raman T_x, the result of the lattice wave modulation of the hyperfine interaction through the admixture of $1S$ doublet states, is in good agreement with the experimental T_x's for the different donors. $1/T_x$ can have an exponential temperature-dependent term but the numerical values suggest it will always be smaller than the T^7 term.

VII. THE LEVEL WIDTH AND SPONTANEOUS PHONON EMISSION

Kane[40] has pointed out that, due to weakness of the electron-phonon interaction in Si, the width of the excited-state impurity levels is determined by the lifetime broadening of the excited states as a result of spontaneous phonon emission rather than by the mechanism of Lax and Burstein.[41] Expressions for the lifetime limited widths of the $1S$ valley-orbit states for intravalley H^{01} and intervalley H^{01} have already been developed in (32) and (34), respectively. These widths have been calculated using $\Xi_u=8.5$ eV, $C_{k_0}{}^0\simeq1$, $C_{k_0}{}^1\sim0.5$, $\bar{v}_l=5.42\times10^5$ cm/sec, $\bar{v}_l=9.33\times10^5$ cm/sec, $v_{t[100]}=5.87\times10^5$ cm/sec, and $v_{l[100]}=8.5\times10^5$ cm/sec. For the longitudinal intervalley W^{sp}, the factor $\sigma(\Xi_d/\Xi_u)$ mentioned in (34) has been explicitly left in the results shown in Table V. For P we note that the contribution to the width Γ due to N processes is probably larger than that due to U processes, whereas for As the bulk of the contribution will be due to U processes unless $\sigma<0.01$. In addition, the doublet states are more important than the triplet states for P while for As the two are equally important.

TABLE V. W^{sp} for $1S$ excited states, in units of 10^{10} sec^{-1}.

Donor and state	$W_t{}^N$	$W_t{}^N$	$W_l{}^U$	$W_t{}^U$	$W_{total}{}^{sp}$
P doublet	1.26	0.74	0.55σ	0.55	≥2.55
P triplet	···	···	0.55σ	0.55	$0.55(1+\sigma)$
As doublet	0.13	···	13.5σ	···	$0.13+13.5\sigma$
As triplet	···	···	13.5σ	···	13.5σ

We now investigate the intervalley differential spontaneous transition probability dW^{sp}/dz where $z=\cos\theta$ and θ is the angle between $\mathbf{q}$ and the [100] axis associated with $\mathbf{K}_\nu$. The factor $|f^z(\mathbf{q}-q_u\hat{z})|^2$ plotted as a function of $\cos\theta$ will vary from $1/\alpha^4$ for $\cos\theta=0$ to $4.3\times10^5/\alpha^4$ for $\cos\theta=1$ if $|\mathbf{q}|=q_\Delta\simeq q_u$. Since $q_\Delta\simeq q_u$ for As, $dW_{50}{}^U/dz$ will be very strongly peaked along both the positive and negative q_z axis. Putting in numbers for As($q_\Delta=q_u$) shows that 40% of $W_{50}{}^U$ will result from q's within a cone $\theta<5.7°$ and a cone $\pi-5.7°<\theta<\pi$. $dW_{10}{}^U/dz$ and $dW_{20}{}^U/dz$ are also strongly dependent on the orientation of $\mathbf{q}$ but have similar peaks along several [100] axis. Since, for As, $W^U\gg W^N$, the above implies that As donor electrons in $1S$ doublet or triplet states decay with the emission of phonons directed primarily along [100] axis. This suggests that if the As donor electrons could somehow be rapidly pumped into these $1S$ excited states it might be possible to generate enough incoherent phonons of frequency 4.8×10^{12} cps to exceed the thermal phonons at $\hbar\omega\sim\Delta$ if it were done at liquid-He temperatures. However, the propagation of such short-wavelength phonons ($\lambda\sim18$ Å) any distance would require very perfect, ultrapure, strain-free material. The detection of these incoherent phonons might be accomplished by several methods, including, for example, the enhancement of the exponential temperature-dependent spin-lattice relaxation rate of As donor electrons.

ACKNOWLEDGMENTS

The author would like to thank G. Feher and E. A. Gere and also G. Ludwig for supplying the samples which made this work possible. He would also like to

[40] E. O. Kane, Phys. Rev. **119**, 40 (1960).
[41] M. Lax and E. Burstein, Phys. Rev. **100**, 592 (1955).

thank Miss E. Krieger for running the computer calculations. Finally, the author is very grateful to F. Ham, W. Harrison, and T. O. Woodruff for stimulating discussions and several helpful suggestions concerning the calculations.

APPENDIX

Orbit-Lattice Matrix Elements and Angular Averages

The absorption orbit-lattice matrix elements between the 1S orbital states are listed below in three separate categories, namely, the long-wavelength region [Eq. (18), $f(q)\simeq 1$], the short-wavelength intravalley matrix elements [Eq. (18)], and the short-wavelength intervalley matrix elements [Eq. (19)].

1. Long-wavelength region

$$\begin{aligned}
&H_{00}^{o1}=(\Xi_d+\tfrac{1}{3}\Xi_u)q_l a_q C_{k_0}^0,\\
&H_{11}^{o1}=[(\Xi_d+\tfrac{1}{6}\Xi_u)q_l+\tfrac{1}{2}\Xi_u e_z q_z]a_q C_{k_0}^0,\\
&H_{22}^{o1}=[(\Xi_d+\tfrac{1}{2}\Xi_u)q_l-\tfrac{1}{2}\Xi_u e_z q_z]a_q C_{k_0}^0,\\
&H_{10}^{o1}=(1/2\sqrt{3})\Xi_u(q_l-3e_z q_z)a_q C_{k_0}^0,\\
&H_{20}^{o1}=(1/\sqrt{6})\Xi_u(e_x q_x-e_y q_y)a_q C_{k_0}^0,\\
&H_{21}^{o1}=(1/\sqrt{2})H_{20}^{o1}.
\end{aligned}\tag{A1}$$

2. Short-wavelength region, intravalley

Since the dominant relaxation ($\hbar\omega\sim\Delta$) occurs with H^{sf} as the middle term we need consider only H_{10}^{o1} and H_{20}^{o1}.

$$\begin{aligned}
H_{01}^{o1}&=(\sqrt{2}/6)\Xi_u[e_x q_x f^x(\mathbf{q})+e_y q_y f^y(\mathbf{q})1\\
&\qquad -2e_z q_z f^z(\mathbf{q})]a_q C_{k_0}^0,
\end{aligned}\tag{A2}$$

$$H_{20}^{o1}=(1/\sqrt{6})\Xi_u[e_x q_x f^x(\mathbf{q})-e_y q_y f^y(\mathbf{q})]a_q C_{k_0}^0.$$

3. Short wavelength, intervalley

$$\begin{aligned}
H_{10}^{o1}&=(1/6\sqrt{2})\{[\Xi_d q_l\pm\Xi_u e_x q_x][f^x(\mathbf{q}+q_u\hat{x})\\
&\quad+f^x(\mathbf{q}-q_u\hat{x})]+[\cdots e_y q_y][f^y(\mathbf{q}+q_u\hat{y})+\cdots]\\
&\quad-2[\cdots e_z q_z][f^z(\mathbf{q}+q_u\hat{z})+\cdots]\}a_q C_{k_0}^1,
\end{aligned}\tag{A3}$$

$$\begin{aligned}
H_{20}^{o1}&=(1/2\sqrt{6})\{[\Xi_d q_l+\Xi_u e_x q_x]\\
&\quad\times[f^x(\mathbf{q}+q_u\hat{x})+f^x(\mathbf{q}-q_u\hat{x})]\\
&\quad-[\cdots e_y q_y][f^y(\mathbf{q}+q_u\hat{y})+\cdots]a_q C_{k_0}^1,\\
H_{30}^{o1}&=(1/2\sqrt{3})\{[\Xi_d q_l+\Xi_u e_x q_x][f^x(\mathbf{q}+q_u\hat{x})\\
&\quad-f^x(\mathbf{q}-q_u\hat{x})]\}a_q C_{k_0}^1,
\end{aligned}$$

H_{40}^{o1} and H_{50}^{o1} same as H_{30}^{o1} replacing x with y and z, respectively.

We now evaluate the solid angle average of $|H^{o1}|^2$, namely $\langle|H^{o1}|^2\rangle_{\Omega_q}$ for the above matrix elements. q_l indicates longitudinal phonons and the other quantities must be averaged over both longitudinal and transverse phonons. For a phonon with propagation vector $\mathbf{q}$ with components $q_x=q\sin\theta\cos\phi$, $q_y=q\sin\theta\sin\phi$, and $q_z=q\cos\theta$, the polarization components are shown below

	Londitudinal	Transverse	Transverse
e_x	$\sin\theta\cos\phi$	$\sin\phi$	$-\cos\theta\cos\phi$
e_y	$\sin\theta\sin\phi$	$-\cos\phi$	$-\cos\theta\sin\phi$
e_z	$\cos\theta$	0	$\sin\theta$

Performing the averages it is readily demonstrated that

$$\langle|H_{m0}^{o1}H_{n0}^{o1}|\rangle=\delta_{mn}.\tag{A4}$$

The results we need for the calculations are:

1. Long-wavelength region

$$\begin{aligned}
\langle|H_{10}^{o1}|^2\rangle&=\langle|H_{20}^{o1}|^2\rangle=2\langle|H_{21}^{o1}|^2\rangle=2\langle|H_{11}^{o1}-H_{00}^{o1}|^2\rangle\\
&=2\langle|H_{22}^{o1}-H_{00}^{o1}|^2\rangle=\sqrt{2}\langle|H_{21}^{o1}H_{20}^{o1}|\rangle\\
&=(2\pi/9)\Xi_u^2 a_q^2\left(\frac{6}{5}q_t^2+\frac{4}{5}q_l^2\right)(C_{k_0}^0)^2.
\end{aligned}$$

2. Short-wavelength region, intravalley

For simplicity we set $f^x=f^y=f^z=f=1/[1+\frac{1}{4}(qa^*)^2]^2$.

$$\begin{aligned}
\langle|H_{10}^{o1}|^2\rangle&=\langle|H_{20}^{o1}|^2\rangle\\
&=(2\pi/9)\Xi_u^2 a_q^2\left[\frac{6}{5}q_t^2 f^2(q_t)+\frac{4}{5}q_l^2 f^2(q_l)\right](C_{k_0}^0)^2.
\end{aligned}$$

3. Short-wavelength region, intervalley, $|\mathbf{q}|\simeq q_\Delta=\Delta/\hbar v$. The functions $f^i(\mathbf{q}\pm q_u\mathbf{i})$ only peak along the ith axis and the solid angle average of all cross terms $f^i f^j$, $i\neq j$, will be negligible. Furthermore, cross terms between opposite valleys will be negligible. With these approximations the angular averages are

$$\begin{aligned}
\langle|H_{\substack{m0\\ m=1\to5}}^{o1}|^2\rangle&=(2\pi/6)\{[\Xi_d^2 I_l^0+2\Xi_d\Xi_u I_l^2+\Xi_u^2 I_t^2]q_{\Delta l}^2\\
&\quad+\Xi_u^2(I_t^2-I_t^4)q_{\Delta t}^2\}a_q^2(C_{k_0}^1)^2,
\end{aligned}$$

where

$$I^n=\frac{1}{\alpha^4}\int_{-1}^{1}\frac{x^n dx}{[1+\beta x-\gamma x^2]^4},$$

with

$$\begin{aligned}
&\alpha=1+\tfrac{1}{4}a^2(q_\Delta^2+\xi q_u^2),\quad \xi=b^2/a^2=0.32,\\
&\beta=(1/\alpha)(\tfrac{1}{2}a^2\xi q_\Delta q_u),\quad a=25\times10^{-8}\text{ cm},\\
&\gamma=(1/\alpha)(\tfrac{1}{4}a^2(1-\xi)q_\Delta^2).
\end{aligned}$$

The I_l^n and I_t^n are evaluated using $q_{\Delta l}$ and $q_{\Delta t}$, respectively. Typical values of I^n are shown below in Table VI.

TABLE VI. Integral for intervalley $\langle|H^{o1}|^2\rangle_{\Omega_q}$.

q_Δ	I^0	I^2	I^4	$f^2(q_\Delta)$
0.20	0.0023	0.0021	0.0019	0.00160
0.22	0.0035	0.0032	0.0030	0.00086
0.345	0.0092	0.0089	0.0086	0.00006

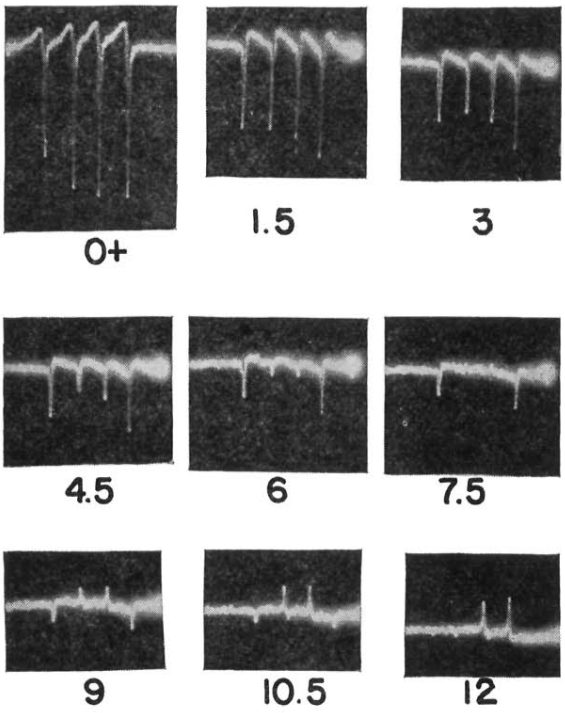

FIG. 8. The recovery of the four As hyperfine lines after inversion of all four lines at 2.44°K (times are in minutes). The unequal signal intensities of the four lines at $t=0$ is mainly a result of an inadequate wait in preparing thermal equilibrium populations.

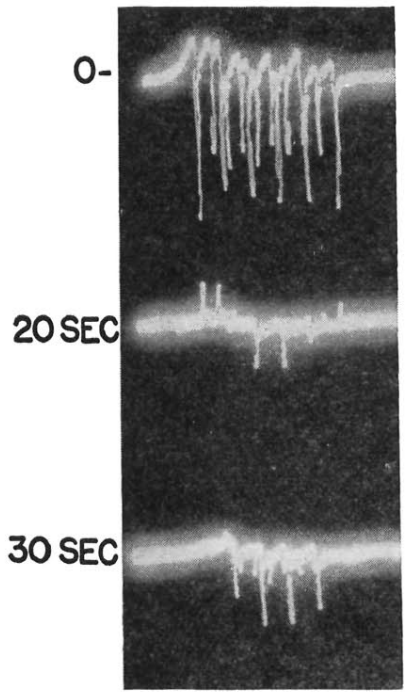

FIG. 9. The recovery after inversion at 2.50°K of the six Sb^{121} hyperfine lines and the eight Sb^{123} hyperfine lines. The Sb^{121} lines are recovering more rapidly than the Sb^{123} lines. For Sb^{121}, $T_z < T_s$ and the central lines are recovering most rapidly because of the dominant hyperfine spin-lattice relaxation.